A Reformulation of Degree of Disequilibrium Analysis for Automatic Selection of Kinetic Constraints in the Rate-Controlled Constrained-Equilibrium Method

Fatemeh Hadi[1]
Dena Scientific,
Wellesley, MA 02482
e-mail: fatemeh.hadi@denasci.com

Shrabanti Roy
Department of Mechanical Engineering,
Mississippi State University,
Starkville, MS 39762
e-mail: sr1937@msstate.edu

Omid Askari
Department of Mechanical Engineering,
Mississippi State University,
Starkville, MS 39762
e-mail: askari@me.msstate.edu

Gian Paolo Beretta
Department of Mechanical and Industrial Engineering,
Università di Brescia,
via Branze, 38, 25123, Brescia, Italy
e-mail: gianpaolo.beretta@unibs.it

The rate-controlled constrained equilibrium (RCCE) is a model reduction scheme for chemical kinetics. It describes the evolution of a complex chemical system with acceptable accuracy with a number of rate controlling constraints on the associated constrained-equilibrium states of the system, much lower than the number of species in the underlying detailed kinetic model (DKM). Successful approximation of the constrained-equilibrium states requires accurate identification of the constraints. One promising procedure is the fully automatable Approximate Singular Value Decomposition of the Actual Degrees of Disequilibrium (ASVDADD) method that is capable of identifying the best constraints for a given range of thermodynamic conditions and a required level of approximation. ASVDADD is based on simple algebraic analysis of the results of the underlying DKM simulation and is focused on the behavior of the degrees of disequilibrium (DoD) of the individual chemical reactions. In this paper, we introduce an alternative ASVDADD algorithm. Unlike the original ASVDADD algorithm that require the direct computation of the DKM-derived DoDs and the identification of the set of linearly independent reactions, in the alternative algorithm, the components of the overall degree of disequilibrium vector can be computed directly by casting the DKM as an RCCE simulation considering a set of linearly independent constraints equaling the number of chemical species in size. The effectiveness and robustness of the derived constraints from the alternative procedure is examined in hydrogen/oxygen and methane/oxygen ignition delay simulations and the results are compared with those obtained from DKM. [DOI: 10.1115/1.4050815]

Keywords: rate-controlled constrained equilibrium (RCCE), dimension reduction for chemical kinetics, singular value decomposition (SVD), derived kinetics constraints

1 Introduction

An important issue in quantitative prediction of turbulent combustion is realistic description of combustion chemistry. Consideration of chemical kinetics in sufficient detail, typically involving hundreds of species and thousands of reaction steps, is however computationally intractable in turbulent flow simulations. To alleviate this issue, significant efforts have been devoted toward development of methods to simplify detailed kinetics as summarized in Ref. [1]. Among the promising methods developed thus far, the rate-controlled constrained equilibrium (RCCE) is particularly appealing due to its basis in classical thermodynamics. This method is originally introduced by Keck and Gillespie [2,3] and further developed and applied by Metghalchi and co-workers [4–19]. The method is also employed in many investigations afterwards [8,9,11,12,20–26]. In RCCE, the evolution of a reacting system is approximated by assuming that the governing detailed kinetic model (DKM) separates the overall chemical dynamics into fast and slow effects. The slow ones are characterized by a relatively small number of slowly varying linear combinations of the species concentrations called RCCE kinetic constraints. The fast ones produce a most rapid local maximization of the entropy compatible with the conservation principles augmented by the RCCE constraints, because on the time scale of the fast dynamics they act effectively as additional conserved properties. As a result of the approximation, the system is at any given time in a constrained equilibrium state, which however shifts in time to adjust to the slowly varying (and, hence, rate controlling) RCCE constraints. It is noteworthy that exactly the same modeling approach has been subsequently considered by various authors in the framework of model order reduction strategies for general dynamical systems, where it has been renamed as the "quasi-equilibrium approximation" often resulting in unfortunate overlooks of the preexisting RCCE literature (see e.g. Ref. [27]). As long as the RCCE constraints can be assumed fixed for a given DKM and a given set of initial and boundary conditions, the RCCE constraints identify a low-dimensional manifold in composition space, where the time evolution can be assumed to take place for the chosen level of approximation. As discussed in Ref. [22], it is also noteworthy that this manifold is not invariant under the dynamics generated by the full DKM. But it is invariant under the approximate dynamics generated by (1) using the full DKM to continuously update the slowly changing values of the RCCE constraints and (2) updating the constrained equilibrium state to the new values.

A very important issue in RCCE is selection of constraints. This challenging issue has been addressed in limited investigations.

[1]Corresponding author.

Contributed by the Internal Combustion Engine Division of ASME for publication in the Journal of Energy Resources Technology. Manuscript received January 30, 2021; final manuscript received April 1, 2021; published online May 3, 2021. Assoc. Editor: Reza Sheikhi.

In previous contributions [10,11], the C_1 hydrocarbon fuel oxidation process is studied and a very successful set of structurally valid constraints are developed based on studying oxidation pathways. Algorithms for automated selection of constraints include that developed by Yousefian [21] as well as other methods based on level of importance to identify single species constraints by determining the species governed by fast/slow mechanisms [28]; greedy algorithm [24,29] to select single species constraints by cyclic direct integration of chemical kinetics; time scale analysis [30–32]; and degree of disequilibrium analysis [12,33–37]. The present work focuses on the latter method.

The paper is organized as follows. Fundamentals of RCCE, its constraint potential formulation and an alternative formulation the Approximate Singular Value Decomposition of the Actual Degrees of Disequilibrium (ASVDADD) method for RCCE constraint selection-based degree of disequilibrium (DoD) analysis is presented in Secs. 2 and 3. The results of RCCE application to constant energy/volume homogeneous ignition and combustion of hydrogen and methane for different sets of initial conditions using the derived constraints are provided in Sec. 4 along with a conclusion in Sec. 5.

2 Governing Equations

In a chemically reacting system involving n_s chemical species, consider chemical reactions of the following form:

$$\sum_{j=1}^{n_s} \nu_{j\ell}^{+} Z_j = \sum_{j=1}^{n_s} \nu_{j\ell}^{-} Z_j \quad (\ell = 1, \ldots, n_r) \tag{1}$$

where $\boldsymbol{Z}$ is the vector of chemical species symbols, $\boldsymbol{\nu}^{+}$ and $\boldsymbol{\nu}^{-}$ are $n_s \times n_r$ matrices of stoichiometric coefficients of reactants and products, respectively, and n_r is the number of reactions. In a macroscopically homogeneous and closed system, the evolution of the system is governed by

$$\frac{dY_j}{dt} = S_j(t) \quad \text{with} \quad S_j(t) = \frac{\dot{\omega}_j M_j}{\rho} \quad (j = 1, 2, \ldots, n_s) \tag{2}$$

where ρ is the density of the gas mixture and Y_j, M_j, and $\dot{\omega}_j$ denote mass fraction, molar mass, and net production rate of chemical species j, respectively, with

$$\dot{\omega}_j = \sum_{\ell=1}^{n_r} \nu_{j\ell}\, \Omega_\ell = \sum_{\ell=1}^{n_r} (\nu_{j\ell}^{-} - \nu_{j\ell}^{+})\, \Omega_\ell \tag{3}$$

where $\nu_{j\ell}$ is the net stoichiometric coefficient of species j in reaction ℓ and Ω_ℓ the net rate of reaction ℓ, defined at temperature T in terms of species concentrations $[N_j]$ and forward and backward reaction rate constants $k_\ell^{\pm}(T)$ by

$$\Omega_\ell = k_\ell^{+}(T) \prod_{j=1}^{n_s} [N_j]^{\nu_{j\ell}^{+}} - k_\ell^{-}(T) \prod_{j=1}^{n_s} [N_j]^{\nu_{j\ell}^{-}} \tag{4}$$

together with the principle of detailed balance

$$\frac{k_\ell^{+}(T)}{k_\ell^{-}(T)} = \left(\frac{p_o}{R_u T}\right)^{\nu_\ell} \exp\left(-\frac{\Delta g_\ell^{o}(T)}{R_u T}\right) \tag{5}$$

where $\nu_\ell = \sum_{j=1}^{n_s} \nu_{j\ell}$, $\nu_{j\ell} = \nu_{j\ell}^{-} - \nu_{j\ell}^{+}$, $\Delta g_\ell^{o}(T) = \sum_{j=1}^{n_s} \nu_{j\ell} g_j(T, p_o)$, and p_o, R_u, $g_j(T, p_o)$ are the standard pressure, the universal gas constant, and the Gibbs free energy per unit mole of pure species j at T and p_o, respectively.

The RCCE method provides a reduced representation of the reacting system using n_c scalars that impose constraints on the evolution of the system. The constraints are assumed to be linear combinations of gas mixture species concentrations [2]

$$C_i = \sum_{j=1}^{n_s} a_{ij} \frac{Y_j}{M_j} \quad (i = 1, 2, \ldots, n_c) \tag{6}$$

where C_i and n_c represent the value and the number of constraints. The transformation matrix a_{ij}, a predefined constant here, represents the contribution of the chemical species j to the constraint i. We assume that the first n_e of these linear combinations are the elemental constraints, representing the concentrations of the atomic elements that compose the molecular species in the DKM (a_{ij}^{EL} represents the number of atoms of kind i in chemical species j). Elemental constraints are conserved exactly by any well-defined DKM. The remaining $n_c - n_e$ are the slowly varying RCCE constraints, which according to the RCCE model are approximately conserved on the fast time scale.

Inserting Eq. (2) into Eq. (6) yields the $n_c - n_e$ rate equations for the slowly varying RCCE constraints

$$\frac{dC_i}{dt} = \sum_{j=1}^{n_s} \frac{a_{ij}}{M_j} S_j(t) \quad (i = n_e + 1, 2, \ldots, n_c) \tag{7}$$

In RCCE, Eq. (2) is replaced by Eq. (7) which is advantageous since Eq. (7) includes fewer ordinary differential equations (ODEs) with reduced numerical stiffness.

The constrained-equilibrium composition is specified using the method of undetermined Lagrange multipliers to maximize the entropy subject to the instantaneous values of the energy, the volume, and the constraints [10]. As detailed for example in Refs. [3,13,38–40], this well-known procedure yields

$$\Lambda_j = \sum_{i=1}^{n_c} a_{ij}\, \gamma_i \tag{8}$$

where γ_i is the ith constraint potential and the vector $\boldsymbol{\Lambda}$ of the dimensionless entropic chemical potentials is defined by

$$\Lambda_j = -\frac{\mu_j(T, \rho, \boldsymbol{Y})}{R_u T} \quad (j = 1, 2, \ldots, n_s) \tag{9}$$

As detailed in Sec. 3.1, for an ideal Gibbs–Dalton mixture of ideal gases, from Eqs. (8) and (9) we obtain

$$Y_j^{\mathrm{RCCE}}(t) = \frac{M_j}{\rho} \frac{p_0}{R_u T(t)} \exp\left(-\frac{g_j(T(t), p_o)}{R_u T(t)}\right) \exp\left(-\sum_{i=1}^{n_c} a_{ij} \gamma_i(t)\right) \tag{10}$$

where Y_j^{RCCE} is the mass fraction of species j at the constrained-equilibrium state.

2.1 Rate Equations for the Constraint Potentials.

The constraint potential representation of RCCE is obtained by transforming Eq. (7) into a set of differential equations for the constraint potentials. For prescribed rates of change of the density and the energy (for example, equal to zero if the closed system has fixed volume and heat losses are negligible), the differential equations for the constraint potentials plus the energy balance equation constitute a set of $n_c + 1$ equations describing the time variation of the temperature and the n_c constraint potentials

$$Q_i^c \frac{1}{T}\frac{dT}{dt} + \sum_{k=1}^{n_c} R_{ik}^c \frac{d\gamma_k}{dt} = C_\alpha \frac{1}{\rho}\frac{d\rho}{dt} + \sum_{j=1}^{n_s} \frac{a_{ij}}{M_j} S_j(t) \tag{11a}$$

$$Q^e \frac{1}{T}\frac{dT}{dt} + \sum_{k=1}^{n_c} R_k^e \frac{d\gamma_k}{dt} = \frac{u}{\rho}\frac{d\rho}{dt} + \frac{du}{dt} \tag{11b}$$

where the coefficients are

$$Q_i^c = \sum_{j=1}^{n_s} a_{ij}\frac{Y_j}{M_j}\frac{u_j}{R_uT}; \quad R_{ik}^c = -\sum_{j=1}^{n_s} a_{ij}a_{kj}\frac{Y_j}{M_j}$$
$$Q^e = c_vT + \sum_{j=1}^{n_s}\frac{u_j^2}{R_uT}\frac{Y_j}{M_j}; \quad R_k^e = -\sum_{j=1}^{n_s} a_{kj}u_j\frac{Y_j}{M_j} \tag{12}$$

where u_j, u, and c_v denote the internal energy per unit mole of pure species j, the specific internal energy per unit mass of the mixture, and the specific heat capacity of the mixture at constant volume, respectively. Notice that since chemical reactions conserve the atomic elements, the second term on the right-hand side of Eq. (11*a*) is different from zero only for $i = n_e + 1, 2, \ldots, n_c$ and, therefore, needs not be computed for ($i = 1, 2, \ldots, n_e$). Given an initial thermodynamic state ($T(0)$,$\gamma_1(0)$,…,$\gamma_{n_c}(0)$), Eq. (11) are integrated to obtain $T(t)$ and $\gamma_k(t)$ ($k = 1, \ldots, n_c$). When substituted into Eq. (10), these variables provide the mass fractions of all the species present in the chemical mechanism.

More general RCCE constraint potential formulations for open systems or for prescribed enthalpy and pressure are given in Refs. [13,35,38,39,41].

3 Constraint Identification Based on Degree of Disequilibrium Analysis and the ASVDADD Algorithm

In this paper, the RCCE constraint selection is focused on the behavior of the degrees of disequilibrium of the individual chemical reactions introduced in Refs. [12,33]. This methodology consists of a straightforward algebraic analysis of the results of probe simulations based on the underlying DKM. In particular, we focus on the variation of this methodology that computes an Approximate Singular Value Decomposition of the Actual Degrees of Disequilibrium (ASVDADD) [33] to find a low dimensional subspace in chemical potential space (the space spanned by the vector $\boldsymbol{\Lambda}$) approximating the actual chemical potential and DoD traces with a given accuracy.

3.1 Original ASVDADD Algorithm.

In the following, a brief summary of the ASVDADD algorithm is given.

I - In the matrix of stoichiometric coefficients $\nu_{j\ell}$ ($j = 1, \ldots, n_s$, $\ell = 1, \ldots, n_r$), a set of $r = n_s - n_e$ linearly independent columns $\boldsymbol{\nu}_{\ell_k}$ ($k = 1, \ldots, r$) is identified.

II - The DoD of reaction ℓ is related to the matrix of stoichiometric coefficients and the chemical potentials of the chemical species in the gas mixture as follows:

$$\phi_\ell(t) = -\frac{1}{R_uT(t)}\sum_{j=1}^{n_s}\nu_{j\ell}\,\mu_j(T(t),\rho,\boldsymbol{Y}(t)) \quad (\ell = 1, 2, \ldots, n_r) \tag{13}$$

where for an ideal Gibbs-Dalton mixture of ideal gases the chemical potentials are related to the mass fractions Y_j by

$$\mu_j(T,\rho,\boldsymbol{Y}) = g_j(T,p_o) + R_uT\ln\frac{\rho R_uT}{p_o} + R_uT\ln\frac{Y_j}{M_j} \tag{14}$$

where, again, g_j is the Gibbs free energy of pure species j.

Equation (13) indicates that the DoD of any chemical reaction ℓ can be viewed as the scalar product

$$\phi_\ell = \sum_{j=1}^{n_s}\Lambda_j\nu_{j\ell} = \langle\boldsymbol{\Lambda}\mid\boldsymbol{\nu}_\ell\rangle \quad (\ell = 1, 2, \ldots, n_r) \tag{15}$$

of the ℓth column $\boldsymbol{\nu}_\ell$ of the stoichiometric matrix $\boldsymbol{\nu}$ and vector of the dimensionless entropic chemical potentials $\boldsymbol{\Lambda}$. The dimensionless vector $\boldsymbol{\Lambda}$ can be decomposed [33,35] as

$$\boldsymbol{\Lambda} = \boldsymbol{\Lambda}_{\mathrm{DoD}} + \boldsymbol{\Lambda}_\perp \tag{16}$$

into the sum of two orthogonal components that lie in the two orthogonal subspaces of $\mathbb{R}^{n_s}$ often referred to as the "reactive subspace" and the "inhert subspace" denoted, respectively, as span($\{\boldsymbol{\nu}_\ell\}$) and span($\{\boldsymbol{a}_i^{\mathrm{EL}}\}$) because one is the $(n_s - n_e)$-dimensional linear span of the columns of the stoichiometric matrix and the other the n_e-dimensional linear span of the columns of the transposed of the matrix a_{ij}^{EL} defining the elemental constraints. The orthogonality of the two subspaces is guaranteed by element conservation which can be written as

$$\langle\boldsymbol{a}_i^{\mathrm{EL}}\mid\boldsymbol{\nu}_\ell\rangle = 0 \quad (i = 1, \ldots, n_e;\ \ell = 1, \ldots, n_r) \tag{17}$$

and, therefore, also implies that $\langle\boldsymbol{\Lambda}_\perp\mid\boldsymbol{\nu}_\ell\rangle = 0$ for every ℓ and that

$$\phi_\ell = \langle\boldsymbol{\Lambda}_{\mathrm{DoD}}\mid\boldsymbol{\nu}_\ell\rangle \quad (\ell = 1, 2, \ldots, n_r) \tag{18}$$

For this reason, $\boldsymbol{\Lambda}_{\mathrm{DoD}}$ is named the Overall Degree of Disequilibrium vector (ODoD). It is the projection of the vector of dimensionless entropic chemical potentials, $\boldsymbol{\Lambda}$, onto the column space of the overall stoichiometric matrix $\boldsymbol{\nu}$, or, that is the same, onto the subspace orthogonal to the elemental constraints $\boldsymbol{a}_i^{\mathrm{EL}}$. This projection can be obtained by either of the following equivalent ways.

II.I—Starting from the degrees of disequilibrium ϕ_k of a set of linearly independent reactions, the ODoD vector $\boldsymbol{\Lambda}_{\mathrm{DoD}}$ can be obtained using the relation [33]

$$\boldsymbol{\Lambda}_{\mathrm{DoD}} = \sum_{k=1}^{r}\phi_k\sum_{k'=1}^{r}W_{kk'}\boldsymbol{\nu}_{\ell_{k'}} \tag{19}$$

where $r = n_s - n_e$, ϕ_k denotes the DoD of the kth linearly independent reaction with stoichiometric vector $\boldsymbol{\nu}_{\ell_k}$, and $\boldsymbol{W} = \boldsymbol{M}^{-1}$ is the inverse of the $r \times r$ matrix $\boldsymbol{M}$ whose components are calculated using $M_{kk'} = \langle\boldsymbol{\nu}_{\ell_k}\mid\boldsymbol{\nu}_{\ell_{k'}}\rangle$. Matrix $\boldsymbol{M}$ is non-singular because of the linear independence of the vectors $\boldsymbol{\nu}_{\ell_k}$, which from a basis for the reactive subspace.

II.II—Starting from the vector $\boldsymbol{\Lambda}$ of the dimensionless entropic potentials Λ_j, the ODoD vector $\boldsymbol{\Lambda}_{\mathrm{DoD}}$ can be obtained using the relation [35]

$$\boldsymbol{\Lambda}_{\mathrm{DoD}} = \boldsymbol{\Lambda} - \boldsymbol{\Lambda}_\perp \tag{20a}$$

where

$$\boldsymbol{\Lambda}_\perp = \sum_{i=1}^{n_e}\gamma_i^{\mathrm{EL}}\boldsymbol{a}_i^{\mathrm{EL}} \tag{20b}$$

$$\gamma_i^{\mathrm{EL}} = \sum_{k=1}^{n_e}(\boldsymbol{G}^{-1})_{ik}\langle\boldsymbol{a}_k^{\mathrm{EL}}\mid\boldsymbol{\Lambda}\rangle \tag{20c}$$

and $\boldsymbol{G}^{-1}$ is the inverse of the positive definite Gram matrix with elements

$$G_{ik} = \langle\boldsymbol{a}_i^{\mathrm{EL}}\mid\boldsymbol{a}_k^{\mathrm{EL}}\rangle \tag{20d}$$

For a generic linear-algebra proof of the construction of the projection (here, $\boldsymbol{\Lambda}_{\mathrm{DoD}}$) of a vector (here, $\boldsymbol{\Lambda}$) onto the subspace orthogonal to the span of a set of linearly independent but not necessarily orthogonal vectors (here the $\boldsymbol{a}_k^{\mathrm{EL}}$'s), see, e.g., the Appendix of Ref. [42].

III—Use DKM derived values of $\boldsymbol{\Lambda}_{\mathrm{DoD}}$ at n_m discrete times t_m and store the data in the $n_s \times n_m$ matrix $\boldsymbol{D}$ with elements

$$D_{jm} = \Lambda_{\mathrm{DoD},j}(t_m) \quad (j = 1, \ldots, n_s;\ m = 1, \ldots, n_m) \tag{21}$$

where m labels the computational time grid points and we assume that $n_m > n_s$.

IV—Compute the Singular Value Decomposition (SVD) of the matrix $\boldsymbol{D}$,

$$\boldsymbol{D} = \boldsymbol{U}\Sigma\boldsymbol{V}^T \tag{22}$$

where $\boldsymbol{U}$ is an $n_s \times n_s$ orthogonal matrix of rank r, $\boldsymbol{V}^T$ is an $n_m \times n_m$ orthonormal matrix also of rank r, and Σ is a $n_s \times n_m$ diagonal matrix having the singular values σ_i of matrix $\boldsymbol{D}$ in decreasing order as the first r elements of the diagonal, i.e., for $k = 1, \ldots, r$, and zeros elsewhere. The singular values σ_i are the positive square roots of the r positive eigenvalues σ_i^2 of the positive semi-definite matrices $\boldsymbol{D}\boldsymbol{D}^T$ and $\boldsymbol{D}^T\boldsymbol{D}$. Since only the first r columns of $\boldsymbol{U}$ matrix are in the column space of $\boldsymbol{D}$, and only the first r rows of $\boldsymbol{V}^T$ matrix (i.e., the first r columns of $\boldsymbol{V}$ matrix) are in the row space of $\boldsymbol{D}$, Eq. (22) can be replaced by the "reduced SVD" form

$$\boldsymbol{D} = \tilde{\boldsymbol{U}}\tilde{\Sigma}\tilde{\boldsymbol{V}}^T \tag{23}$$

where $\tilde{\boldsymbol{U}}$ is the $n_s \times r$ orthogonal matrix made up of the first r columns of $\boldsymbol{U}$, $\tilde{\boldsymbol{V}}^T$ is the $r \times n_m$ made up of the first r rows of $\boldsymbol{V}^T$, and $\tilde{\Sigma}$ is the $r \times r$ diagonal matrix with the r singular values σ_i in decreasing order on the diagonal.

Now, defining $\tilde{\boldsymbol{\gamma}} = \tilde{\Sigma}\tilde{\boldsymbol{V}}^T$, Eq. (23) becomes

$$D_{jm} = \sum_{i=1}^{r} U_{ji}\,\sigma_i\,V_{mi} = \sum_{i=1}^{r} U_{ji}\,\tilde{\gamma}_{im} \tag{24}$$

or, equivalently, denoting the columns of $\tilde{\boldsymbol{U}}$ by $\tilde{\boldsymbol{u}}_k$,

$$\boldsymbol{\Lambda}_{\mathrm{DoD}}(t_m) = \sum_{i=1}^{r} \tilde{\boldsymbol{u}}_i\,\tilde{\gamma}_i(t_m) \tag{25}$$

Equation (25) shows that the time evolution $\boldsymbol{\Lambda}_{\mathrm{DoD}}(t_m)$ of the ODoD vector resulting from the solution of the full DKM lies in the r-dimensional subspace of $\mathbb{R}^{n_s}$ spanned by the columns $\tilde{\boldsymbol{u}}_i$ of $\tilde{\boldsymbol{U}}$.

But a strength of the SVD stems from the Eckert–Young theorem [43] which constitutes the basis of the ASVDADD algorithm [33,35]. It states that the "best" approximate time evolution lying in a lower dimensional subspace of $\mathbb{R}^{n_s}$ is obtained by simply truncating the sum in Eq. (25). Thus, choosing any n_c with $n_c - n_e < r$, the best approximate time evolution lying in an $(n_c - n_e)$-dimensional subspace is given by

$$\boldsymbol{\Lambda}_{\mathrm{DoD}}^{\mathrm{approx}}(t_m)\big|_{(n_c-n_e)\text{-dim}} = \sum_{i=1}^{n_c-n_e} \tilde{\boldsymbol{u}}_i\,\tilde{\gamma}_i(t_m) \tag{26}$$

V—Next we observe that within the RCCE model Eq. (10) inserted into Eq. (14) and then in Eq. (9) yields $\Lambda_j^{\mathrm{RCCE}} = \sum_{i=1}^{n_c} a_{ij}\,\gamma_i$ or, equivalently, $\boldsymbol{\Lambda}^{\mathrm{RCCE}} = \sum_{i=1}^{n_c} \boldsymbol{a}_i\,\gamma_i$ so that its projection onto the reactive subspace is

$$\boldsymbol{\Lambda}_{\mathrm{DoD}}^{\mathrm{RCCE}} = \sum_{i=n_e+1}^{n_c} \gamma_i\,\boldsymbol{a}_i \tag{27}$$

Therefore, comparison of Eqs. (26) and (27) indicates that the "best" $n_c - n_e$ RCCE kinetic constraints (in addition to the n_e elemental constraints) are the first $n_c - n_e$ columns of $\tilde{\boldsymbol{U}}$, which is the ASVDADD recipe for RCCE constraint selection

$$\boldsymbol{a}_i^{\mathrm{ASVDADD}} = \begin{cases} \boldsymbol{a}_i^{\mathrm{EL}} & i = 1, \ldots, n_e \\ \tilde{\boldsymbol{u}}_{i-n_e} & i = n_e + 1, \ldots, n_c \end{cases} \tag{28}$$

Considering that all we need are the columns of the SVD matrix $\boldsymbol{U}$, it is noteworthy that they are the left-singular vectors of matrix $\boldsymbol{D}$ and form a set of orthonormal eigenvectors of matrix $\boldsymbol{D}\boldsymbol{D}^T$ whose eigenvalues are the squares of the singular values of $\boldsymbol{D}$. Therefore, the ASVDADD constraints can also be found by solving the eigenvalue problem for matrix $\boldsymbol{D}\boldsymbol{D}^T$.

VI—As a result, the constraint Eqs. (6) are set as follows:

$$C_i^{\mathrm{EL}} = \sum_{j=1}^{n_s} a_{ij}^{\mathrm{EL}}\,\frac{Y_j}{M_j} \quad (i = 1, \ldots, n_e) \tag{29a}$$

$$C_i = \sum_{j=1}^{n_s} U_{(i-n_e)j}\,\frac{Y_j}{M_j} \quad (i = n_e + 1, \ldots, n_c) \tag{29b}$$

Note that if we choose $n_c = n_e + r = n_s$ the RCCE model considers all the r columns of matrix $\tilde{\boldsymbol{U}}$ as kinetic constraints, and, therefore, it involves no approximation: for the same initial conditions, it yields the exact DKM solution. The number of kinetic constraints can be decreased by abandoning the last $n_e + r - n_c = n_s - n_c$ columns of matrix $\tilde{\boldsymbol{U}}$, giving rise to a hierarchy of RCCE approximate solutions of decreasing accuracy with respect to the exact DKM solution.

3.2 Inclusion of Prescribed Constraints. In the RCCE literature, some constraints have been identified on the basis of important kinetic considerations, for example, the total number of moles is often considered a rate controlling constraint based on the general observation that it is conserved by two-body reactions and only the much slower three-body reactions can change it.

The ASVDADD approach can be readily adapted to a set of n_p (linearly independent) prescribed constraints $\boldsymbol{a}_q^{\mathrm{PC}}$, with $q = 1, 2, \ldots, n_p$, by simply "appending" them to the set of elemental constraints $\boldsymbol{a}_i^{\mathrm{EL}}$, so that the linear span of the augmented set is $n_e + n_p$-dimensional. More explicitly, Eq. (20) then become

$$\boldsymbol{\Lambda}_{\mathrm{DoD}} = \boldsymbol{\Lambda} - \boldsymbol{\Lambda}_{\perp} \tag{30a}$$

where

$$\boldsymbol{\Lambda}_{\perp} = \sum_{i=1}^{n_e+n_p} \gamma_i^{\mathrm{EL+PC}}\boldsymbol{a}_i^{\mathrm{EL+PC}} \tag{30b}$$

$$\gamma_i^{\mathrm{EL+PC}} = \sum_{k=1}^{n_e+n_p} (\boldsymbol{G}^{-1})_{ik}\langle \boldsymbol{a}_k^{\mathrm{EL+PC}} | \boldsymbol{\Lambda} \rangle \quad i = 1, \ldots, n_e + n_p \tag{30c}$$

$$\boldsymbol{a}_i^{\mathrm{EL+PC}} = \begin{cases} \boldsymbol{a}_i^{\mathrm{EL}} & i = 1, \ldots, n_e \\ \boldsymbol{a}_{i-n_e}^{\mathrm{PC}} & i = n_e + 1, \ldots, n_e + n_p \end{cases} \tag{30d}$$

and $\boldsymbol{G}^{-1}$ is the inverse of the positive definite Gram matrix with elements

$$G_{ik} = \langle \boldsymbol{a}_i^{\mathrm{EL+PC}} | \boldsymbol{a}_k^{\mathrm{EL+PC}} \rangle \tag{30e}$$

In this case, the vector $\boldsymbol{\Lambda}_{\mathrm{DoD}}$ evolves in the $(n_s - n_e - n_p)$-dimensional subspace of $\mathbb{R}^{n_s}$ orthogonal to the elemental and the prescribed constraints, which for the particular case when the total number of moles is the only prescribed constraint, is the linear span of the stoichiometric vectors $\boldsymbol{\nu}_\ell$ of the two-body reactions in the DKM. Equation (28) extends as follows:

$$\boldsymbol{a}_i^{\mathrm{ASVDADD}} = \begin{cases} \boldsymbol{a}_i^{\mathrm{EL}} & i = 1, \ldots, n_e \\ \boldsymbol{a}_{i-n_e}^{\mathrm{PC}} & i = n_e + 1, \ldots, n_e + n_p \\ \tilde{\boldsymbol{u}}_{i-n_e-n_p} & i = n_e + n_p + 1, \ldots, n_c \end{cases} \tag{31}$$

3.3 Alternative ASVDADD Algorithm. Alternatively to steps II.I and II.II above, which require the direct computation of the DKM-derived DoDs and the identification of the set of linearly independent reactions, the components of the $\boldsymbol{\Lambda}_{\mathrm{DoD}}$ vector can be computed directly by casting the DKM as an RCCE simulation with the following set of n_s linearly independent constraints

$$C_i^{\mathrm{EL+PC}} = \sum_{j=1}^{n_s} a_{ij}^{\mathrm{EL+PC}}\,\frac{Y_j}{M_j} \quad (i = 1, \ldots, n_e + n_p) \tag{32a}$$

$$C_i = \sum_{j=1}^{n_s} \delta_{ij}\,\frac{Y_j}{M_j} \quad (i = n_e + n_p + 1, \ldots, n_s) \tag{32b}$$

Notice that the $n_s \times n_s$ matrix $\boldsymbol{a}^*$ of constraint coefficients, defined by the elements

$$a^*_{ij} = a^{\mathrm{EL+PC}}_{ij} \quad \text{for } i = 1, \ldots, n_e + n_p \text{ and } a^*_{ij} = \delta_{ij} \text{ for } i = n_e + n_p + 1, \ldots, n_s \tag{33}$$

is invertible owing to the linear independence of the constraints. Denoting its inverse matrix by $\boldsymbol{a}^{-1}_*$, we may invert Eq. (8) to yield

$$\gamma^*_i = \sum_{i=1}^{n_s} \Lambda^*_j \, (\boldsymbol{a}^{-1}_*)_{ji} \tag{34}$$

In this way, the DKM model can be replaced by a fully equivalent RCCE model with n_s constraints, obtained by considering as constraints, in addition to the $n_e + n_p$ elemental plus prescribed constraints, the mole fractions of the last $n_s - n_e - n_p$ species in the species list. Different orderings of the species list give different RCCE models that are all fully equivalent to the DKM model provided that the mole fractions are initially all nonvanishing. Otherwise, exact equivalence is obtained by replacing the vanishing initial mole fractions with very small values, say 10^{-20}, for both the RCCE and DKM simulation.

At this stage, we may proceed in two equivalent ways. The first is to run the DKM starting from the slightly modified initial conditions, to obtain the time dependences of the temperature, $T^*(t)$, and of the mass fractions $Y^*_j(t)$. These, inserted in Eq. (14) yield the time dependence of the chemical potentials and hence of the entropic chemical potentials $\Lambda^*_j(t)$, which in turn, using Eq. (34) give the constraint potentials $\gamma^*_i(t)$. The second route is to solve Eqs. (11) for the above equivalent RCCE simulation with n_s constraints, defined by Eqs. (32), to obtain directly the time dependences of the temperature, $T^*(t)$, and of the constraint potentials $\gamma^*_k(t)$, which inserted in Eq. (8) yield the entropic chemical potentials $\Lambda^*_j(t)$.

From the $\gamma^*_i(t)$'s and Eq. (30*b*), we obtain the time dependences $\Lambda^*_{\perp j}(t) = \sum_{k=1}^{n_e+n_p} \gamma^*_k(t)\, a^*_{kj}$ of the components of vector $\boldsymbol{\Lambda}^*_\perp(t)$, so that finally, using Eq. (30*a*), we obtain the ODoD vector

$$\boldsymbol{\Lambda}^*_{\mathrm{DoD}}(t) = \boldsymbol{\Lambda}^*(t) - \sum_{i=1}^{n_e+n_p} \gamma^*_i(t)\, \boldsymbol{a}^{\mathrm{EL+PC}}_i \tag{35}$$

which can then be subjected to the SVD as described in steps III–VI above.

A noteworthy advantage of the particular set of constraints defined by Eqs. (32) and (33) is that we can write

$$\Lambda^*_j(t) = \sum_{i=1}^{n_e+n_p} \gamma^*_i(t)\, a^{\mathrm{EL+PC}}_{ij} + \sum_{i=n_e+n_p+1}^{n_s} \gamma^*_i(t)\, \delta_{ij} \tag{36}$$

which compared with Eq. (35) shows that vector $\boldsymbol{\Lambda}^*_{\mathrm{DoD}}(t)$ has only $r' = n_s - n_e - n_p$ nonzero components,

$$\Lambda^*_{\mathrm{DoD},j}(t) = \gamma^*_j(t) \text{ for } j > n_e + n_p \text{ whereas } \Lambda^*_{\mathrm{DoD},j}(t) = 0 \text{ for } j \le n_e + n_p \tag{37}$$

allowing the following simplification of the SVD computation in steps III–VI.

In fact, using the values of $\boldsymbol{\Lambda}^*_{\mathrm{DoD}}$ at n_m discrete time instants t_m, the matrix $\boldsymbol{D}$ defined in step III has entries in the first $n_e + n_p$ rows that are all zero. Therefore, the SVD can be conveniently applied to the $r' \times n_m$ submatrix $\boldsymbol{D}^*$ defined by the elements

$$D^*_{jm} = \Lambda^*_{\mathrm{DoD},n_e+n_p+j}(t_m) \quad (j = 1, \ldots, r' = n_s - n_e - n_p;\ \ m = 1, \ldots, n_m) \tag{38}$$

so that

$$\boldsymbol{D}^* = \boldsymbol{U}^* \Sigma^* \boldsymbol{V}^{*T} \tag{39}$$

where $\boldsymbol{U}^*$ is an $r' \times r'$ orthogonal full rank matrix, $\boldsymbol{V}^{*T}$ is an $n_m \times n_m$ orthonormal matrix also of rank r', and Σ^* is an $r' \times n_m$ diagonal matrix having the singular values σ^*_i of matrix $\boldsymbol{D}^*$ in decreasing order on the diagonal of the left $r' \times r'$ square submatrix and zero entries in all columns between $r'+1$ and n_m. Note that all r' columns of matrix $\boldsymbol{U}^*$ are in the column space of $\boldsymbol{D}^*$ but only the first r' rows of $\boldsymbol{V}^{*T}$ (or the first r' columns of $\boldsymbol{V}^*$) are in the row space of $\boldsymbol{D}^*$. This means that Eq. (39) can be replaced by the "reduced SVD"

$$\boldsymbol{D}^* = \boldsymbol{U}^* \tilde{\Sigma}^* \tilde{\boldsymbol{V}}^{*T} \tag{40}$$

As before $\tilde{\boldsymbol{V}}^{*T}$ is an $r' \times n_m$ matrix, and $\tilde{\Sigma}^*$ is $r' \times r'$ diagonal.

Finally, to obtain the $n_s \times r'$ matrix $\tilde{\boldsymbol{U}}^*$ whose columns $\tilde{\boldsymbol{u}}_k$ are the ASVDADD constraints as defined in steps IV and V, we "mount" again, on top of the square matrix $\boldsymbol{U}^*$, the $n_e + n_p$ rows with all entries equal to zero. Then, Eq. (28), i.e., the ASVDADD recipe for RCCE constraint selection, extends as follows. For an RCCE model with n_c constraints, the "best" $n_c - n_e - n_p$ kinetic constraints, additional to the $n_e + n_p$ elemental plus prescribed constraints, are the first $n_c - n_e - n_p$ columns of $\tilde{\boldsymbol{U}}^*$,

$$\boldsymbol{a}^{\mathrm{ASVDADD}*}_i = \begin{cases} \boldsymbol{a}^{\mathrm{EL}}_i & i = 1, \ldots, n_e \\ \boldsymbol{a}^{\mathrm{PC}}_{i-n_e} & i = n_e + 1, \ldots, n_e + n_p \\ \tilde{\boldsymbol{u}}^*_{i-n_e-n_p} & i = n_e + n_p + 1, \ldots, n_c \end{cases} \tag{41}$$

For every choice of n_c, the sets of constraints obtained by Eqs. (41) and (31) are different. But in A, we prove that they are entirely equivalent in that they span exactly the same n_c-dimensional subspace of $\mathbb{R}^{n_s}$, in other words, we prove that the columns of $\boldsymbol{a}^{\mathrm{ASVDADD}*}$ are linear combinations of those of $\boldsymbol{a}^{\mathrm{ASVDADD}}$ (and viceversa).

The effectiveness and robustness of RCCE models based on the ASVDADD constraint selection procedure is demonstrated in Refs. [33–35] for several simulations of increasing difficulty including (1) a one-dimensional expansion of the products of the hydrogen/oxygen combustion in a supersonic nozzle ($n_s = 8$ species, $n_e = 2$ elements, $n_r = 24$ reactions); (2) methane/oxygen combustion in the same supersonic nozzle ($n_s = 29$ species, $n_e = 3$ elements, $n_r = 133$ reactions); and (3) ignition delay simulation of homogeneous methane/air mixture ($n_s = 53$ species, $n_e = 5$ elements, $n_r = 325$ reactions).

4 Results

In this section, we present and discuss ignition delay simulations of H_2/O_2 and CH_4/O_2 mixtures in a constant energy/volume perfectly stirred reactor (PSR) for different initial pressures and temperatures. The assumed DKM for the H_2/O_2 mixture includes $n_s = 8$ species, $n_e = 2$ elements, and the $n_r = 24$ reaction steps [12] listed in Table 1 where the $r = n_s - n_e = 6$ linearly independent reactions chosen for use in Eq. (19) are $\ell_k = 1, 11, 12, 13, 14, 20$ with $k = 1, \ldots, 6$.

4.1 RCCE Simulations. First, we considered a 3×3 grid consisting of the following three temperatures and three pressures: (1660 K, 1310 K, 1080 K) and (100 atm, 10 atm, 1 atm) for the H_2/O_2 mixture. These values are evenly distanced on a log (p) versus $1/T$ scale. Tables 2–5 list the six derived constraints and the constraint-related singular values for the initial conditions of ($p = 1$ atm and $T = 1660$ K), ($p = 100$ atm and $T = 1660$ K), ($p = 1$ atm and $T = 1080$ K), and ($p = 100$ atm and $T = 1080$ K), respectively. The sum of the six derived constraints and the two chemical element constraints form the maximum number of constraints available for RCCE simulations, which is 8. In order to see the effect of number of constraints used, RCCE simulations were performed for

Table 1 H_2/O_2 detailed kinetics model

ℓ	Reaction ℓ	A_ℓ^+	b_ℓ^+	E_ℓ^+
1	$O + O + M = O_2 + M$	1.20E + 17	−1	0
2	$O + H + M = OH + M$	5.00E + 17	−1	0
3	$H + H + M = H_2 + M$	1.00E + 18	−1	0
4	$H + H + H_2 = H_2 + H_2$	9.00E + 16	−0.6	0
5	$H + H + H_2O = H_2 + H_2O$	6.00E + 19	−1.3	0
6	$H + OH + M = H_2O + M$	2.20E + 22	−2	0
7	$H + O_2 + M = HO_2 + M$	2.80E + 18	−0.9	0
8	$H + O_2 + O_2 = HO_2 + O_2$	2.08E + 19	−1.2	0
9	$H + O_2 + H_2O = HO_2 + H_2O$	1.13E + 19	−0.8	0
10	$OH + OH + M = H_2O_2 + M$	7.40E + 13	−0.4	0
11	$O + H_2 = H + OH$	3.87E + 04	2.7	6260
12	$O + HO_2 = OH + O_2$	2.00E + 13	0	0
13	$O + H_2O_2 = OH + HO_2$	9.63E + 06	2	4000
14	$H + O_2 = O + OH$	2.65E + 16	−0.7	17,041
15	$H + HO_2 = O + H_2O$	3.97E + 12	0	671
16	$H + HO_2 = O_2 + H_2$	4.48E + 13	0	1068
17	$H + HO_2 = OH + OH$	8.40E + 13	0	635
18	$H + H_2O_2 = HO_2 + H_2$	1.21E + 07	2	5200
19	$H + H_2O_2 = OH + H_2O$	1.00E + 13	0	3600
20	$OH + H_2 = H + H_2O$	2.16E + 08	1.5	3430
21	$OH + OH = O + H_2O$	3.57E + 04	2.4	−2110
22	$OH + HO_2 = O_2 + H_2O$	1.45E + 13	0	−500
23	$OH + H_2O_2 = HO_2 + H_2O$	2.00E + 12	0	427
24	$HO_2 + HO_2 = O_2 + H_2O_2$	1.30E + 11	0	−1630

Note: The units of A_ℓ^+ and E_ℓ^+ for use in Eq. (4) for $k_\ell^+(T) = A_\ell^{+b_\ell^+} \exp(-E_\ell^+/R_uT)$ are mole-cm-s-K and cal/mol, respectively. The six linearly independent reactions chosen for use in Eq. (19) are reactions 1, 11, 12, 13, 14 and 20.

three sets of derived constraints. In the first, the four constraints with the largest singular values were selected, in the second the first 3, and in the third only, the first 2, resulting, respectively, in a total of 6, 5, and 4 constraints. The simulation results are shown in Figs. 1(*a*), 2(*a*), and 3(*a*) where DKM and RCCE predicted ignition temperatures are compared. Results show excellent agreement between DKM and RCCE predicted temperatures, when six total constraints are used (not shown in the figures). In these simulations, the maximum difference in predicted RCCE and DKM ignition delay times of all the cases is 3.5%. The ignition delay time is defined as the time needed for 10% rise over the initial temperature. Considering the uncertainties inherent in thermochemical parameters used in these computations, it is reasonable to consider these differences as insignificant and hence assume that only two derived constraints are needed for accurate RCCE simulation of temperature when constraints are obtained for individual cases.

The Eckart–Young theorem says that $\|\boldsymbol{D}\|_2 = \sigma_1$ and $\|\boldsymbol{D} - \boldsymbol{D}_i\|_2 = \sigma_{i+1}$, where $\|\cdot\|_2$ denotes the spectral norm and $\boldsymbol{D}_i$ is the approximation of $\boldsymbol{D}$ obtained from its SVD truncated by keeping only the first i singular values and setting the others to zero. Therefore, the ratios σ_{i+1}/σ_1 listed in Tables 2–5 represent these errors normalized by the spectral norm of the exact $\boldsymbol{D}$. We see that if we want an overall error of less than 5% in the prediction of the ODoD, the first case requires three constraints, the second, third and fourth require only two constraints which is consistent with the minimum number of constraints required to keep ignition delay time error small. The tables list also the value of the alternative error measure

$$\delta_{\text{Fro},i} = \sqrt{\sum_{k=i+1}^{r} \sigma_k^2} \Big/ \sqrt{\sum_{k=1}^{r} \sigma_k^2} \tag{42}$$

based on the fact that the Eckart–Young theorem also says that $\|\boldsymbol{D}\|_{\text{Fro}} = (\sum_{k=1}^{r} \sigma_k^2)^{1/2}$ and $\|\boldsymbol{D} - \boldsymbol{D}_i\|_{\text{Fro}} = (\sum_{k=i+1}^{r} \sigma_k^2)^{1/2}$ where $\|\cdot\|_{\text{Fro}}$ denotes the Frobenius norm.

The performance of the alternative SVD formulation with and without prescribed constraints is assessed by recalculating RCCE predicted ignition temperatures of the previous cases. These simulations plus the previous ones encompasses four RCCE/SVD models: (1) ASVDADD original model that requires the identification of

Table 2 ASVDADD derived constraints for initial conditions of $p = 1$ atm and $T = 1660$ K

i	H	O	O_2	OH	HO_2	H_2O_2	H_2	H_2O	σ_i	σ_{i+1}/σ_1	$\delta_{\text{Fro},i}$
1	0.4179	0.2269	0.1574	−0.179	0.2002	−0.0526	−0.0526	−0.6581	128.5005	39.36%	37.08%
2	−0.5256	−0.5925	0.1986	−0.348	0.0634	0.3007	0.3007	−0.1848	50.5725	6.36%	6.22%
3	−0.092	−0.1222	0.5041	0.1717	0.0181	−0.6947	−0.6947	0.2957	8.1751	1.82%	1.94%
4	0.2715	−0.59	−0.1842	0.3288	0.5643	−0.1665	−0.1665	−0.166	2.3384	0.95%	0.95%
5	0.3302	−0.3114	0.4137	0.3813	−0.6042	0.251	0.251	−0.1911	1.2183	0.39%	0.36%
6	−0.5037	0.1824	−0.2449	0.6932	−0.0366	0.0098	0.0098	−0.3324	0.5043	0.00%	0.00%

Table 3 ASVDADD derived constraints for initial conditions of $p = 100$ atm and $T = 1660$ K

i	H	O	O_2	OH	HO_2	H_2O_2	H_2	H_2O	σ_i	σ_{i+1}/σ_1	$\delta_{\text{Fro},i}$
1	0.3825	0.1941	0.1565	−0.2089	0.2172	−0.0328	0.5045	−0.6672	60.6634	23.95%	23.45%
2	−0.5535	−0.5823	0.3709	−0.256	−0.0296	0.1056	0.3693	−0.0552	14.5282	2.54%	2.85%
3	0.1461	−0.1097	0.424	0.5311	−0.0465	−0.6639	0.1971	0.1515	1.5412	1.25%	1.43%
4	0.0583	−0.5539	−0.2992	0.48	0.4075	0.1191	−0.2111	−0.3809	0.7595	0.73%	0.74%
5	0.1853	−0.0582	0.266	0.3257	−0.7137	0.4465	−0.08	−0.2651	0.4445	0.22%	0.21%
6	−0.6197	0.4437	-0.285	0.4347	−0.0591	0.0082	0.3204	−0.2065	0.1331	0.00%	0.00%

Table 4 ASVDADD derived constraints for initial conditions of $p = 1$ atm and $T = 1080$ K

i	H	O	O_2	OH	HO_2	H_2O_2	H_2	H_2O	σ_i	σ_{i+1}/σ_1	$\delta_{\text{Fro},i}$
1	0.3384	0.1564	0.1195	−0.2995	0.2331	0.0594	0.4855	−0.6808	136.7955	12.65%	13.20%
2	−0.5492	−0.5297	0.4518	−0.1888	−0.0602	−0.0509	0.4129	0.0371	17.3016	4.13%	4.12%
3	0.2062	0.1433	0.3608	0.6157	−0.1575	−0.5835	0.2499	0.0013	5.6562	0.37%	0.46%
4	−0.0855	−0.5123	−0.3184	0.475	0.5381	−0.0419	−0.1035	−0.3183	0.5008	0.27%	0.28%
5	0.4518	−0.4622	0.3126	0.1409	−0.446	0.3932	−0.2682	−0.1984	0.3663	0.08%	0.08%
6	−0.4751	0.3071	−0.1891	0.4083	−0.3976	0.4047	0.179	−0.3516	0.1094	0.00%	0.00%

Table 5 ASVDADD derived constraints for initial conditions of $p = 100$ atm and $T = 1080$ K

i	H	O	O_2	OH	HO_2	H_2O_2	H_2	H_2O	σ_i	σ_{i+1}/σ_1	$\delta_{Fro,i}$
1	0.3051	0.127	0.1028	−0.357	0.2325	0.1199	0.4703	−0.6805	314.9413	9.26%	9.53%
2	0.5205	0.4889	−0.488	0.0672	0.0472	0.1878	−0.4553	−0.0499	29.1703	2.42%	2.43%
3	0.3326	0.2624	0.2754	0.6001	−0.1085	−0.5672	0.2171	−0.062	7.6358	0.27%	0.28%
4	−0.0558	0.4361	−0.0238	−0.5308	0.2999	−0.4555	0.1452	0.4537	0.8465	0.07%	0.07%
5	0.286	0.1745	0.462	−0.3353	−0.6921	0.2176	−0.0327	0.1858	0.2094	0.03%	0.03%
6	−0.5799	0.5926	−0.2114	0.1744	−0.3037	0.2011	0.2924	−0.139	0.0945	0.00%	0.00%

linearly independent reactions to determine the constraints abbreviated to SVD, henceforth, (2) ASVDADD with prescribed constraints which derives the constraints following ASVDADD approach; however, it only the identification of linearly independent two-body reactions when the molar constraint, which is independent of two-body reactions, is considered as an assigned constraint (abbreviated to SVDP), (3) alternative ASVDADD model that do not require the identification of linearly independent reactions to compute the constraints as a counterpart of the SVD model (abbreviated to ASVD), and (4) alternative ASVDADD model with prescribed constraints as a counterpart of the SVDP model (abbreviated to ASVDP). The simulation results of the SVDP, ASVD, and ASVDP models are shown in Figs. 1–3 where DKM and RCCE predicted ignition temperatures are compared. Ignition delay time error in RCCE simulations with five total constraints is below 5% in all cases; however, the same is not true for SVDP and ASVDP cases with four total constraints in which the error is not acceptable. This result is surprising since SVDP and ASVDP are counterparts to SVD and ASVD with the replacement of one derived constraint with the molar constraint considering its success as a "universal" constraint [10]. Figure 4 shows constraint potentials in exact RCCE simulations with six derived constraints for SVD and ASVD models and with five derived and molar constraints for SVDP and ASVDP models. As can be seen the SVD and ASVD models have two derived constraint potentials with significant non-zero values while it is three for SVDP and ASVDP models which confirms the previous result that for SVDP and ASVDP models a minimum number of five total constraints is necessary for accurate simulations. Figure 5 shows constraint potentials in reduced RCCE simulations with five derived constraints for SVD and ASVD models and with two derived and molar constraints for SVDP and ASVDP models. The consistency in the predictions of the three constraint potentials in the exact simulations SVD(8), SVDP(8), ASVD(8), and ASVDP(8) and the reduced ones SVD(5), SVDP(5), ASVD(5) and ASVDP(5) in Fig. 5 demonstrates the ability of the reduced RCCE model with five total constraints in the accurate prediction of kinetics.

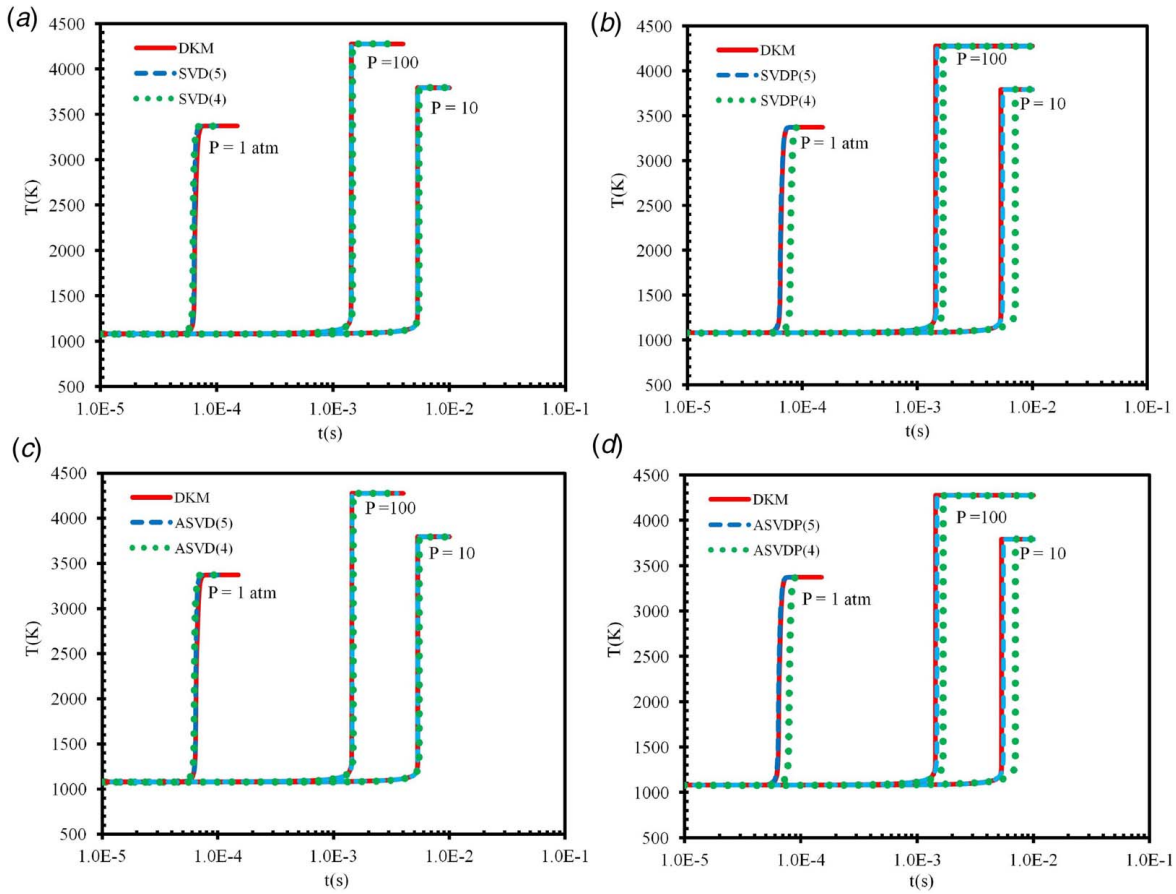

Fig. 1 RCCE and DKM (solid lines) temperature predictions of stoichiometric H_2/O_2 combustion at initial temperature of 1080 K. Total number of constraints for RCCE is 5 (dashed lines) and 4 (dotted lines).

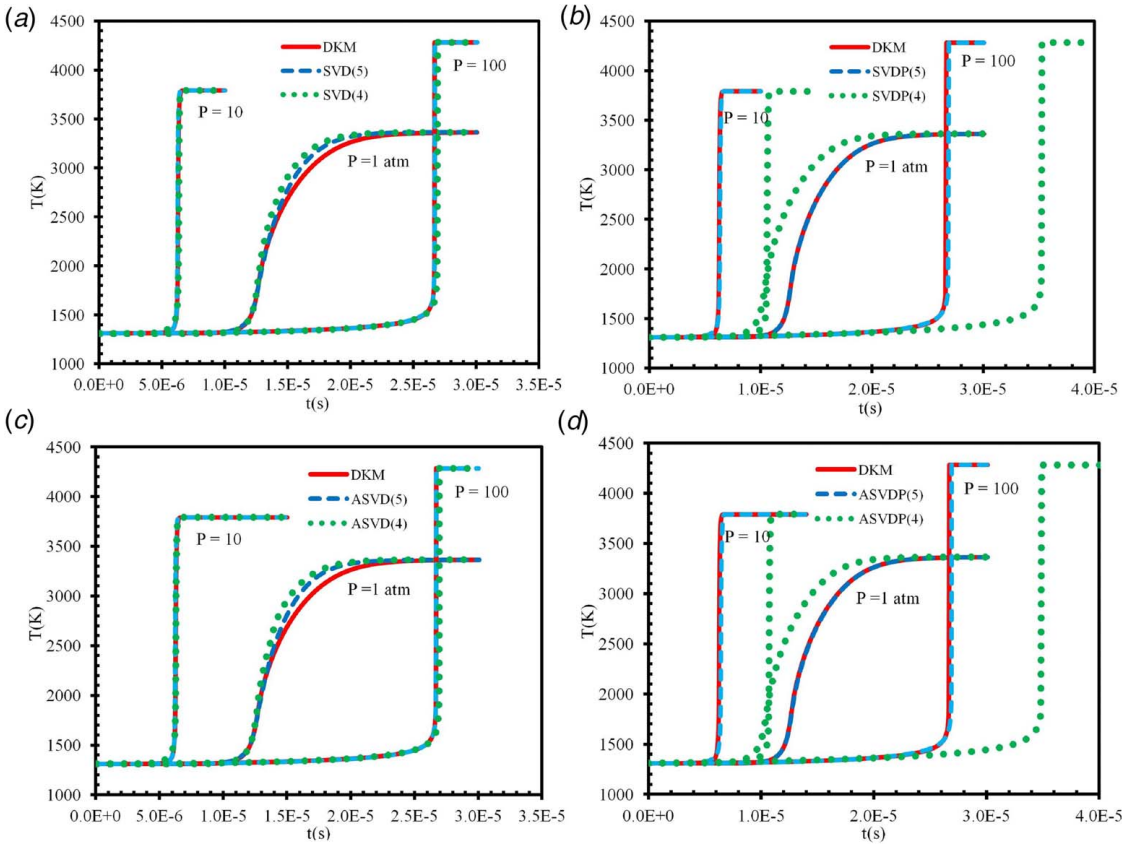

Fig. 2 RCCE and DKM (solid lines) temperature predictions of stoichiometric H_2/O_2 combustion at initial temperature of 1310 K. Total number of constraints for RCCE is 5 (dashed lines) and 4 (dotted lines).

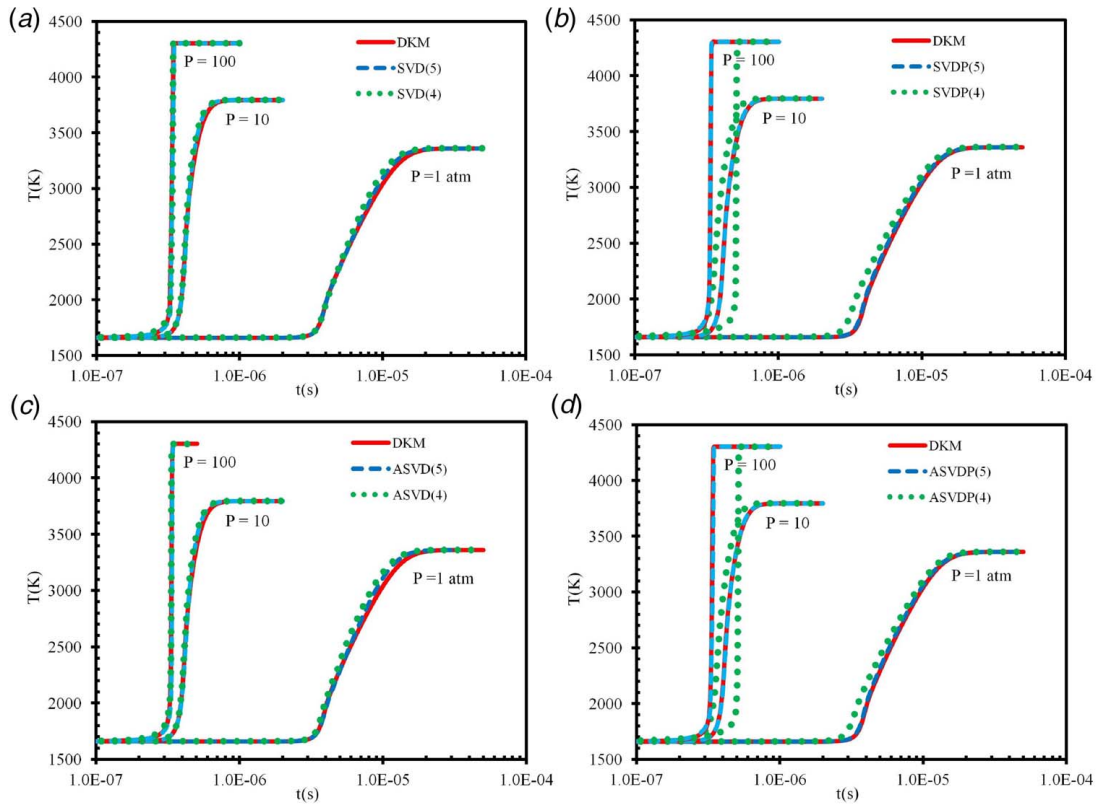

Fig. 3 RCCE and DKM (solid lines) temperature predictions of stoichiometric H_2/O_2 combustion at initial temperature of 1660 K. Total number of constraints for RCCE is 5 (dashed lines) and 4 (dotted lines).

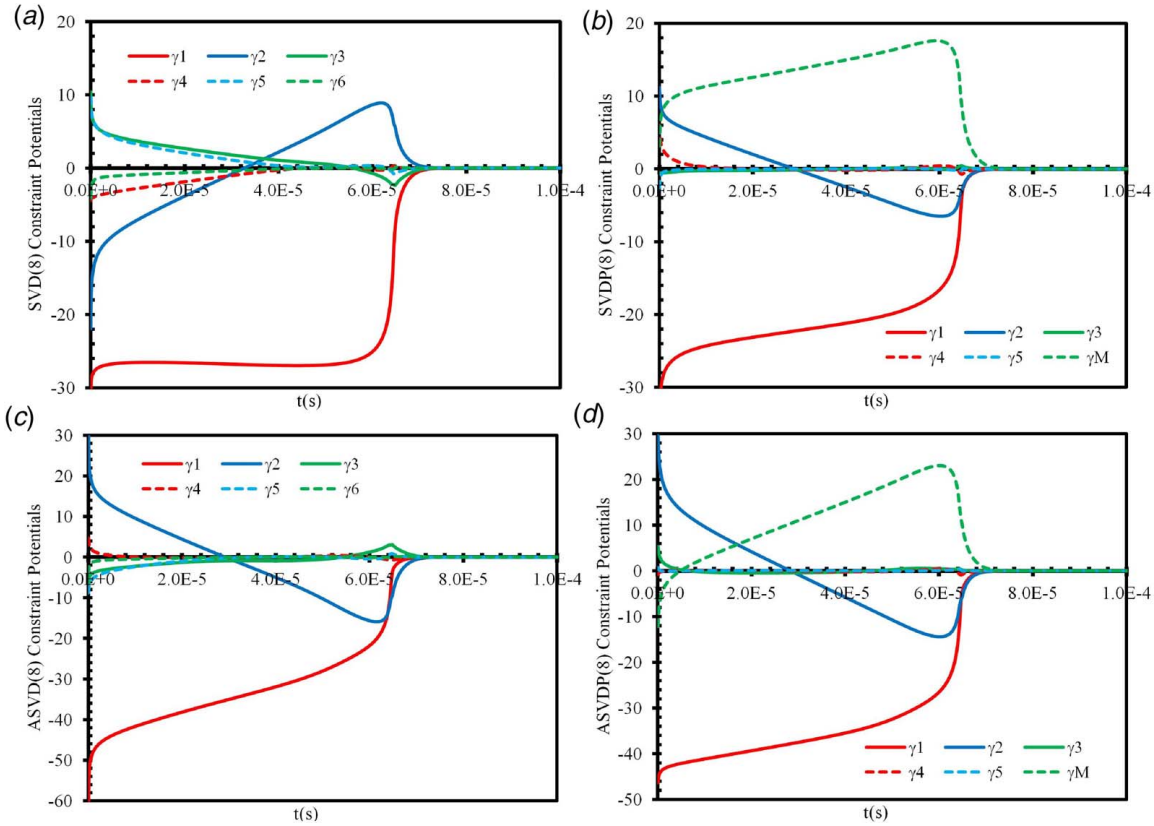

Fig. 4 Constraint potential predictions of stoichiometric H_2/O_2 combustion at initial temperature of 1080 K. Total number of constraints for RCCE is 8.

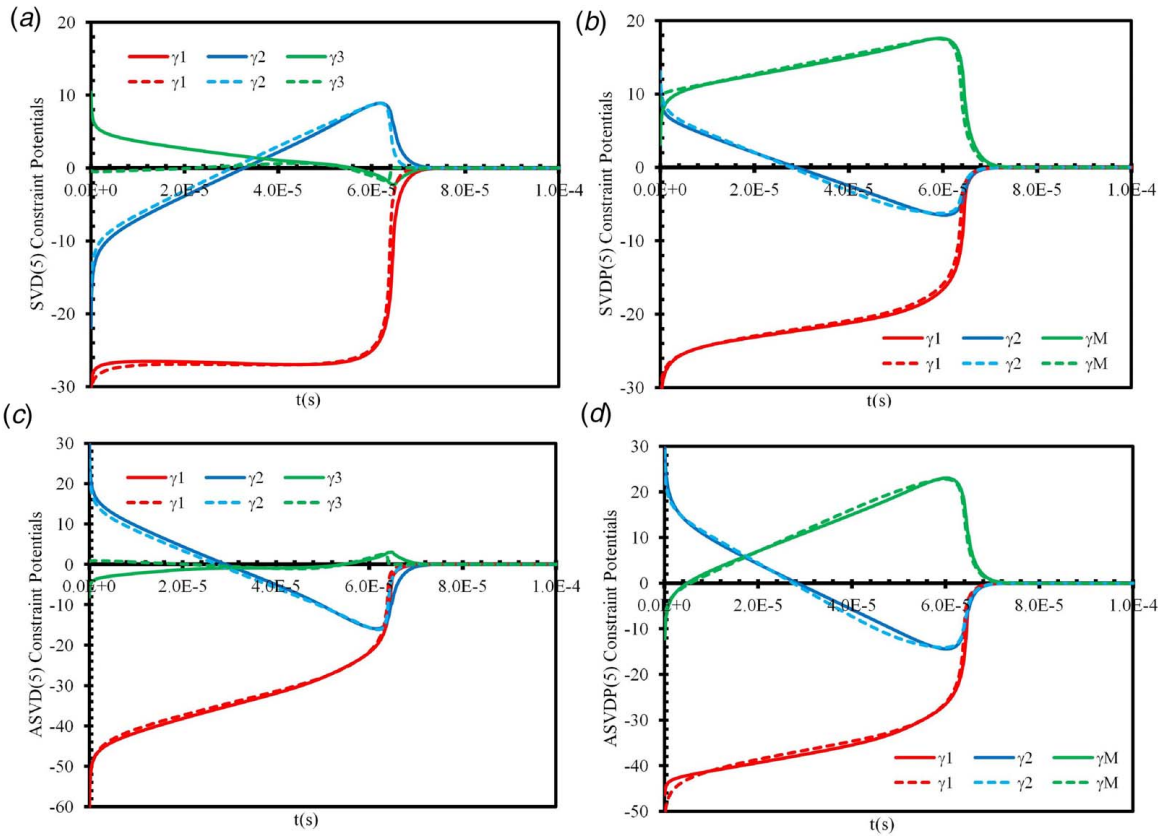

Fig. 5 Comparison of three constraint potentials in exact and reduced RCCE simulations of stoichiometric H_2/O_2 combustion at initial temperature of 1080 K. Total number of constraints is 5 in the reduced RCCE simulation.

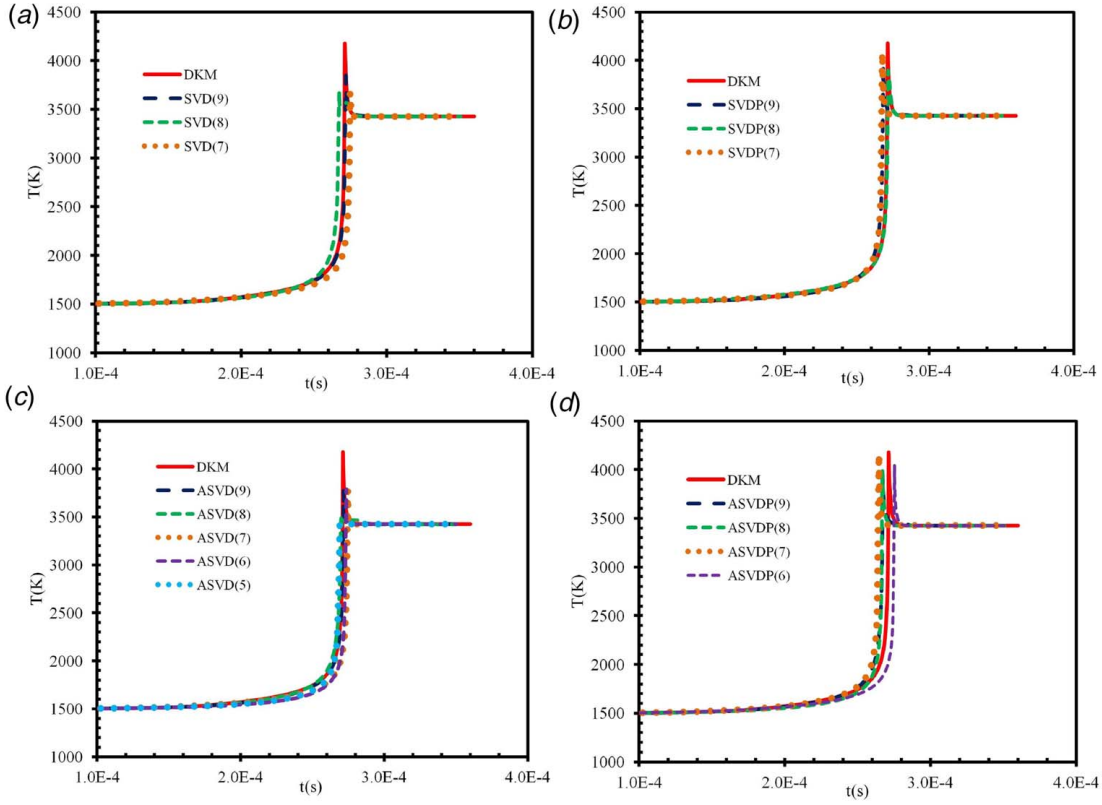

Fig. 6 RCCE and DKM temperature predictions of stoichiometric CH_4/O_2 combustion at initial temperature and pressure of 1500 K and 1.0 atm, respectively, using the 29-species 132-reactions CH_4/O_2 system described in Ref. [10]

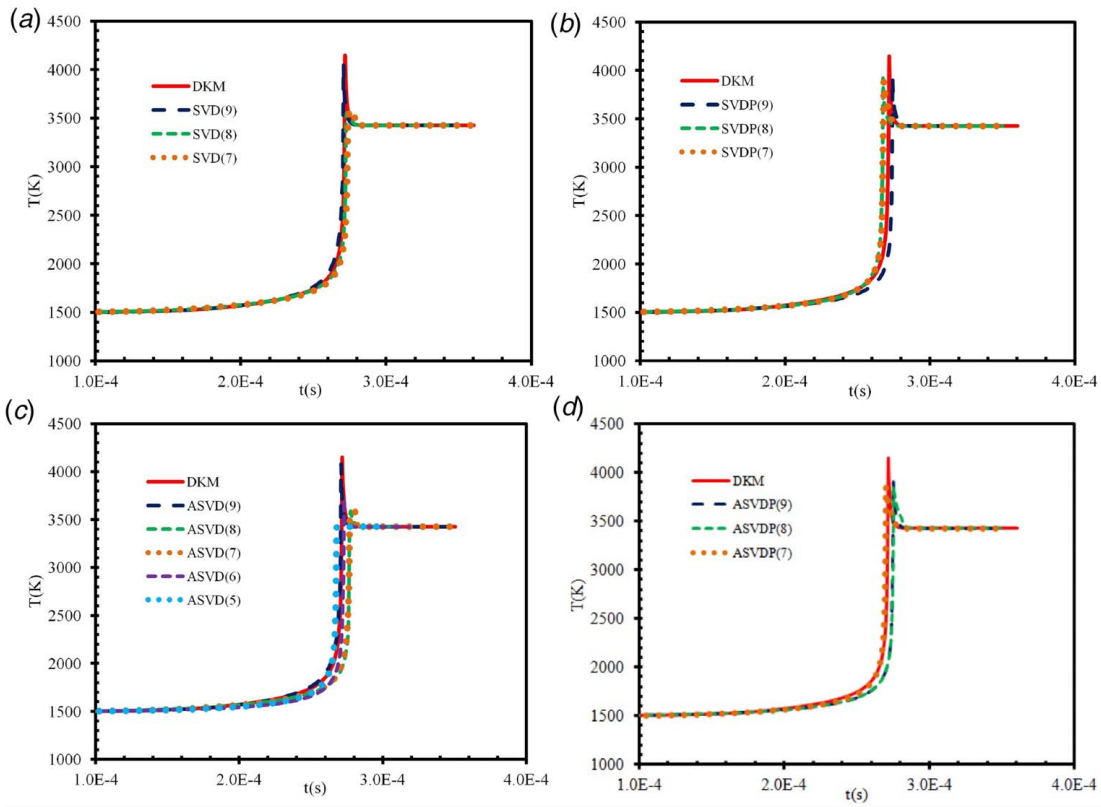

Fig. 7 RCCE and DKM temperature predictions of stoichiometric CH_4/O_2 combustion at initial temperature and pressure of 1500 K and 1.0 atm, respectively, using a 19-species simplified version of CH_4/O_2 system described in Ref. [10]

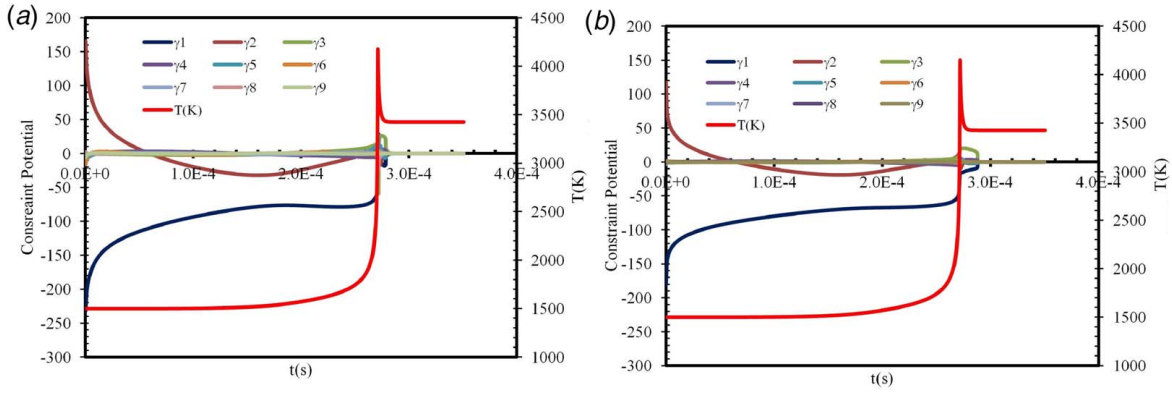

Fig. 8 Constraint potential predictions of stoichiometric CH_4/O_2 combustion at initial temperature and pressure of 1500 K and 1.0 atm, respectively

Figure 6 shows the CH_4/O_2 ignition temperatures simulated by the four SVD models, assuming constant volume and internal energy with initial temperature and pressure of 1500 K and 1.0 atm, respectively. The 29-species 132-reaction CH_4/O_2 system described in Ref. [10] is considered here for the simulations. Also simulated is a 19-species 94-reaction simplified version of this system, with DKM ignition temperatures nearly identical to those of the 29-species system, justifying the exclusion of the 10 neglected species from simulations (Fig. 7). The 10 neglected species are OCHO, HOOCO, OOCHO, HOOCHO, CH_2OOH, HOCHO, HOCO, CH_2, CH, C. Figures 6(*a*), 6(*c*) and 7(*a*), 7(*c*) show that the minimum number of constraints required by SVD and ASVD models to obtain acceptable results is the same for both the 19- and 29-species systems. This also verifies the insignificance of the 10 neglected species in the case considered. To be more specific, in the ASVD(7) case, the seven constraints are the summation of three elemental and four out of 16 SVD derived constraints for the 19-species system and four out of 26 for the 29-species case, which means that the 10 additional SVD constraints not needed in the 29-speceis simulation could be due to the insignificance of the 10 neglected species. Furthermore, the plots of ASVD constraint potentials in Fig. 8 clearly show that in both the 19- and 29- species systems the first two constraint potentials are significantly greater in magnitude than the rest, hence, only the two corresponding constraints are required for ASVD(5) simulations. Unlike the eight-species H_2/O_2 simulations, in this case, the SVD and ASVD simulation results with reduced number of constraints are not exactly the same. Additionally, for the initial conditions considered, the SVD plots in Figs. 6(*a*) and 7(*a*) show that for both the 19- and 29-species systems, this model accurately predicts ignition temperatures with a minimum of seven constraints, which is two more than the number of constraints required by the ASVD model in Figs. 6(*c*) and 7(*c*).

Figures 6(*b*), 6(*d*) and 7(*b*), 7(*d*) show the SVDP and ASVDP simulation results. According to Figs. 6(*b*) and 7(*b*), the minimum number of constraints the SVDP model requires for acceptable simulation for both the 19- and 29- species systems is seven, which is now the summation of three elemental, one molar, and three derived constraints. As Figs. 6(*d*) and 7(*d*) show, however, the ASVDP model, which also includes the molar constraint, requires, respectively, seven and six constraints for the 19- and 29-species systems. This is the only case where additional species seem to make a difference in the results, although, counterintuitively, less number of constraints is required in the 29-species system. It is useful to note that in the SVD simulation models, the constraints whose potentials are negligible in the full simulation are neglected in the reduced simulation. As implied above, the vanishing of certain potentials could be due to the insignificance of certain species. Therefore, it would be interesting to determine whether this is really the case as well as to be able to identify these type of constraints.

In Ref. [44], also for methane, it is shown that adding constraints does not always produce improvement of the temperature profile: going from 7 to 10 to 13 seems to worsen the situation (for ignition time and temperature profile) but 13 does begin capturing the temperature overshoot and 16 improves it. In the same reference, it is also shown that same behavior can be observed for chemical species profiles. For instance, it is shown that OH and CH_3

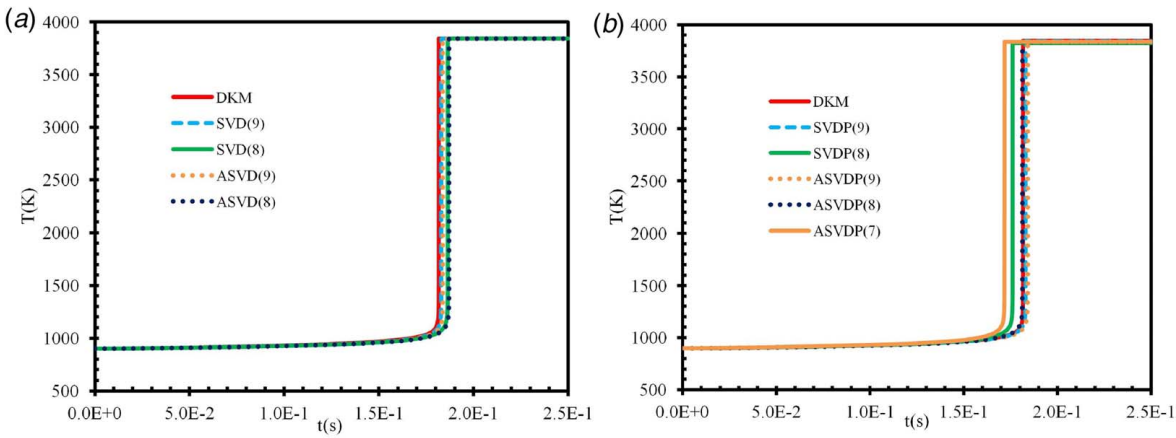

Fig. 9 RCCE and DKM temperature predictions of stoichiometric CH_4/O_2 combustion at initial temperature and pressure of 900 K and 10 atm, respectively

overshoots are captured better by 10 than 13 constraints. Therefore, it is safe to conclude that partial results (temperature, constraint potentials, DoD's of some reactions, mole fractions, etc.) provide only partial aspects, while the ASVDADD method optimizes the overall DoD, whose components are also shown for example, for H_2/O_2, in Ref. [35]. Again, the eight components of the entropic chemical potential reactive subspace, $\mathbf{\Lambda}_{\mathrm{DoD}}$, are partial aspects as well. In other words, the ASVDADD method optimizes the overall distance between $\mathbf{\Lambda}_{\mathrm{DoD}}^{RCCE}$ and $\mathbf{\Lambda}_{\mathrm{DoD}}$, averaged along the time trajectory (with the time average weighted on the time grid chosen by the DKM numerical scheme), so it is difficult to judge improvement even by looking at these components. For just eight of them (such as for the hydrogen case), it is quite apparent that going from three to four to five constraints results in clear improvement. But for methane, the components are many more, and therefore, it may happen that some constraints improve while others worsen the results, somewhat leading to a misjudgment of the average improvement which is granted by the ASVDADD.

The plots in Fig. 9 show the SVD, ASVD, SVDP, and ASVDP simulated ignition temperatures of 29-species CH_4/O_2 system at initial temperature and pressure of 900 K and 10 atm (the 19-species simulation does not apply to this system). As these figures show, with a total of eight constraints, SVD, ASVD, and SVDP models accurately predict the ignition temperatures while the ASVDP model does this with one less constraint.

5 Conclusion

The ASVDADD algorithm, employing DoD analysis of a probe DKM simulation, computes a full spectrum of RCCE constraints that are capable of characterizing the kinetic bottlenecks rate-controlling the underlying DKM in the chosen range of conditions. The ASVDADD method optimizes the overall difference between the average overall degree of disequilibrium obtained from DKM and RCCE by automatically ranking the candidate constraints. In this paper, an alternative to the original ASVDADD algorithm is introduced. The alternative procedure computes the components of the overall degree of disequilibrium vector by casting DKM as an RCCE without requiring the identification of linearly independent reactions. In addition, the new procedure obtains an orthogonal full rank matrix for constraints further simplifying the original algorithm. We have proven that the two algorithms are entirely equivalent mathematically in that they span exactly the same n_c-dimensional subspace of the reactive subspace. However, they result in two different sets of components of the chemical potentials that depend on the linearly independent reactions governing the species chemical evolution. The effectiveness and robustness of the alternative ASVDADD procedure is demonstrated using ignition delay simulation of homogeneous hydrogen/oxygen and methane/oxygen mixtures. The results show that the two methods have comparable accuracy with the alternative ASVDADD algorithm performing slightly better in some of the cases studied.

Acknowledgment

We are grateful to Dr. Vreg Yousefian for countless insightful discussions and help with the formulation and results and for performing the simulations.

Conflict of Interest

There are no conflicts of interest.

Data Availability Statement

The authors attest that all data for this study are included in the paper.

Appendix: Proof of Equivalence of Original and Alternative ASVDADD Algorithms

Let us start by combining Eqs. (30*a*), (25), (35), and (40), to write

$$\mathbf{\Lambda}^*(t) = \sum_{i=1}^{n_e+n_p} \gamma_i^{*\mathrm{EL}+PC}(t)\, \boldsymbol{a}_i^{\mathrm{EL+PC}} + \sum_{i=1}^{r} \tilde{\boldsymbol{u}}_i^*\, \tilde{\gamma}_i^*(t) \tag{A1}$$

$$\mathbf{\Lambda}(t) = \sum_{i=1}^{n_e+n_p} \gamma_i^{\mathrm{EL+PC}}(t)\, \boldsymbol{a}_i^{\mathrm{EL+PC}} + \sum_{i=1}^{r} \tilde{\boldsymbol{u}}_i\, \tilde{\gamma}_i(t) \tag{A2}$$

Next we recall that both algorithms start from the same DKM simulation (or a fully equivalent RCCE simulation with $n_c = n_s$ constraints). Therefore, the resulting base time evolutions of the vector of the entropic chemical potentials are identical, i.e., we have $\mathbf{\Lambda}^*(t) = \mathbf{\Lambda}(t)$, so that Eqs. (A1) and (A2) yield, for every t and hence every t_m,

$$\sum_{i=1}^{r} \tilde{\boldsymbol{u}}_i\, \tilde{\gamma}_i(t_m) = \sum_{i=1}^{r} \tilde{\boldsymbol{u}}_i^*\, \tilde{\gamma}_i^*(t_m) + \sum_{i=1}^{n_e+n_p} [\gamma_i^{*\mathrm{EL}+PC}(t_m) - \gamma_i^{\mathrm{EL+PC}}(t_m)]\, \boldsymbol{a}_i^{\mathrm{EL+PC}} \tag{A3}$$

where (for simplicity) we assume $t_m^* = t_m$, i.e., identical time discretization for the two simulations.

Recalling that, with the SVD in step 4, for $i = 1, \ldots, r$, we defined $\tilde{\gamma}_i(t_m) = \sigma_i V_{mi}$ and similarly defining, for the alternative algorithm, $\tilde{\gamma}_i^*(t_m) = \sigma_i^* V_{mi}^*$, and making use of the orthonormality relations $\sum_{m=1}^{n_m} V_{mi} V_{mk} = \delta_{ik}$ and $\sum_{m=1}^{n_m} V_{mi}^* V_{mk}^* = \delta_{ik}$, we multiply Eq. (A3) by $\sigma_k^{-1} V_{mk}$ and sum over m to obtain

$$\tilde{\boldsymbol{u}}_k = \sum_{i=1}^{r} \tilde{\boldsymbol{u}}_i^*\, c_{ik} + \sum_{i=1}^{n_e+n_p} d_{ik}\, \boldsymbol{a}_i^{\mathrm{EL+PC}} \tag{A4}$$

where,

$$c_{ik} = \sigma_i^* \sigma_k^{-1} \sum_{m=1}^{n_m} V_{mi}^* V_{mk}$$
$$d_{ik} = \sigma_k^{-1} \sum_{m=1}^{n_m} [\tilde{\gamma}_i^{*\mathrm{EL}+PC}(t_m) - \tilde{\gamma}_i^{\mathrm{EL+PC}}(t_m)] V_{mk} \tag{A5}$$

Equation (A4) proves that each vector $\tilde{\boldsymbol{u}}_k$ is a linear combination of the vectors $\tilde{\boldsymbol{u}}_i^*$ and $\boldsymbol{a}_i^{\mathrm{EL+PC}}$. Therefore, they span exactly the same $n_c = r + n_e + n_p$-dimensional subspace of $\mathbb{R}^{n_s}$.

To show the linear relationship between the two models, we additionally consider, as an illustrative example, the dissociation of N_2/O_2 system, with species N, O_2, NO, O and N_2, with molar densities $n_1, n_2, \ldots, n_5$, governed by the five reactions shown in Table 6, three of which are linearly independent. In order to investigate the relationship between the original and alternative ASVDADD algorithms for a reacting system we consider the DKM determined chemical potentials of the species in this system and the identification of linearly independent reactions governing the species

Table 6 N_2/O_2 reacting system

ℓ	Reaction ℓ
1	$NO + O = O_2 + N$
2	$N_2 + O = NO + N$
3	$NO + M = N + O + M$
4	$O_2 + M = O + O + M$
5	$N_2 + M = N + N + M$

Note: The three linearly independent reactions chosen for use in Eq. (19) are reactions 1, 2, and 3.

chemical evolution. Using different algorithms, both models first determine the component of the chemical potentials that depend on these reactions (the projection onto the column space of the matrix of stoichiometric coefficients) and then apply the singular value decomposition technique to approximate this projection which gives the RCCE constraint matrix. The main difference between the two algorithms is the fact that, unlike the ASVD model, the SVD model needs the identification of linearly independent reactions to determine the required component of chemical potentials, resulting in two different sets of such components.

The species chemical potential vector is μ_j ($j=1, \ldots, n_s=5$) and selecting the first three reactions as the linearly independent set, $\nu_{\ell_k}=\boldsymbol{\nu}_I$ ($k=1, \ldots, r=3$), the independent reactions coefficient matrix from the matrix of stoichiometric coefficients $\nu_{j\ell}$ ($j=1, \ldots, 5$, $\ell=1, \ldots, r=5$) is identified:

$$\boldsymbol{\nu}_I=\begin{bmatrix} 1 & 1 & 1 \\ 1 & 0 & 0 \\ -1 & 1 & -1 \\ -1 & -1 & 1 \\ 0 & -1 & 0 \end{bmatrix} \tag{A6}$$

In the SVD model, the component of the entropic chemical potentials that depends on chemical reactions is, as explained before, the projection of this vector onto the column space of the matrix $\nu_{j\ell}$ (which is the same as the column space of the matrix $\boldsymbol{\nu}_I$), can be obtained by using Eq. (19) in which the elements of the vector ϕ_k ($k=1, 2, 3$) are the DoDs of the three independent reactions. Expanding the term containing the stoichiometric matrix, Eq. (19) for the system considered becomes

$$\begin{bmatrix} 0.0571 & 0.343 & 0.429 \\ 0.314 & -0.114 & -0.143 \\ -0.286 & 0.286 & -0.143 \\ -0.343 & -0.0571 & 0.429 \\ 0.114 & -0.314 & -0.143 \end{bmatrix}\begin{bmatrix}\phi_1\\ \phi_2\\ \phi_3\end{bmatrix}=\begin{bmatrix}\Lambda_{\mathrm{DoD}_1}\\ \Lambda_{\mathrm{DoD}_2}\\ \Lambda_{\mathrm{DoD}_3}\\ \Lambda_{\mathrm{DoD}_4}\\ \Lambda_{\mathrm{DoD}_5}\end{bmatrix} \tag{A7}$$

This relation implies that only the first three elements of the vector $\boldsymbol{\Lambda}_{\mathrm{DoD}}$ are needed to determine the relationship between the two models because the remaining two elements can be obtained using the first 3. Let $\boldsymbol{A}_{SVD}$ be the top 3 by 3 matrix of the first matrix on the left-hand side, $\boldsymbol{B}$ the remaining 2 by 3 matrix, $\boldsymbol{\Lambda}_{SVD}$ the three first elements of the vector on the right hand side, and $\boldsymbol{\Lambda}_2$ the remaining 2 element vector. With these definitions, we have $\boldsymbol{\Lambda}_{SVD}=\boldsymbol{A}_{SVD}\boldsymbol{\phi}$ and $\boldsymbol{\Lambda}_2=\boldsymbol{B}\boldsymbol{\phi}$. Substitution of the expression $\boldsymbol{\phi}=\boldsymbol{A}_{SVD}^{-1}\boldsymbol{\Lambda}_{SVD}$ in the last equation yields $\boldsymbol{\Lambda}_2=\boldsymbol{B}\boldsymbol{A}_{SVD}^{-1}\boldsymbol{\Lambda}_{SVD}$. This shows that the elements of $\boldsymbol{\Lambda}_2$ are the linear combination of the 3 independent elements. Since $\boldsymbol{\phi}$ is the same in both SVD and ASVD models, equating this with the one derived next will yield the desired relationship.

Given the DKM determined chemical potential vector, ASVD model identifies its reaction dependent component by considering the following equations, which represent the system's DKM-equivalent RCCE model

$$\boldsymbol{C}=\boldsymbol{a}\boldsymbol{n} \tag{A8a}$$

$$\boldsymbol{\Lambda}=\boldsymbol{a}^T\boldsymbol{\gamma} \tag{A8b}$$

which are Eqs. (6) and (8) in vectorized form. In this model, for the N_2/O_2 system, these are given by

$$\boldsymbol{C}=\begin{bmatrix}n_1\\ n_2\\ n_3\\ C_O\\ C_N\end{bmatrix}\boldsymbol{\gamma}=\begin{bmatrix}\gamma_1\\ \gamma_2\\ \gamma_3\\ \gamma_O\\ \gamma_N\end{bmatrix}\boldsymbol{a}=\begin{bmatrix}1 & 0 & 0 & 0 & 0\\ 0 & 1 & 0 & 0 & 0\\ 0 & 0 & 1 & 0 & 0\\ 0 & 2 & 1 & 1 & 0\\ 1 & 0 & 1 & 0 & 2\end{bmatrix} \tag{A9}$$

C_O and C_N are the molar constraints of O and N elements and γ_O and γ_N their corresponding potentials. With species potential vector given, this relation can be inverted to determine the five elements of constraint potential vector. Since γ_O and γ_N do not explicitly depend on kinetics, $\boldsymbol{\gamma}$ can be decomposed into the sum of the components $\boldsymbol{\gamma}_{ch}$, which depends on chemistry and $\boldsymbol{\gamma}_{el}$, which does not

$$\boldsymbol{\gamma}=\begin{bmatrix}\gamma_1\\ \gamma_2\\ \gamma_3\\ 0\\ 0\end{bmatrix}+\begin{bmatrix}0\\ 0\\ 0\\ \gamma_O\\ \gamma_N\end{bmatrix}\equiv\boldsymbol{\gamma}_{ch}+\boldsymbol{\gamma}_{el} \tag{A10}$$

Using Eq. (A8), $\boldsymbol{\Lambda}_{ch}$ and $\boldsymbol{\Lambda}_{el}$ can be obtained as

$$\boldsymbol{\Lambda}_{ch}=\boldsymbol{a}^T\boldsymbol{\gamma}_{ch} \tag{A11a}$$

$$\boldsymbol{\Lambda}_{el}=\boldsymbol{a}^T\boldsymbol{\gamma}_{el} \tag{A11b}$$

Since $\boldsymbol{\Lambda}_{ch}$ is the only kinetics dependent component and since $\boldsymbol{a}^T\boldsymbol{\gamma}_{ch}=\boldsymbol{\gamma}_{ch}$ using Eqs. (15) and (18), the DoD of this system becomes

$$\boldsymbol{\phi}=\boldsymbol{\nu}_I^T\boldsymbol{\Lambda}=\boldsymbol{\nu}_I^T\boldsymbol{\Lambda}_{ch}=\boldsymbol{\nu}_I^T\boldsymbol{\gamma}_{ch}=\begin{bmatrix}1 & 1 & 1\\ 1 & 0 & 0\\ -1 & 1 & -1\\ -1 & -1 & 1\\ 0 & -1 & 0\end{bmatrix}^T\begin{bmatrix}\gamma_1\\ \gamma_2\\ \gamma_3\\ 0\\ 0\end{bmatrix}$$
$$=\begin{bmatrix}1 & 1 & 1\\ 1 & 0 & 0\\ -1 & 1 & -1\end{bmatrix}^T\begin{bmatrix}\gamma_1\\ \gamma_2\\ \gamma_3\end{bmatrix} \tag{A12}$$

Reference to the constraint vector in Eq. (A9) shows that only the first three elements of this vector depend on kinetics, which means that in this case the coefficient matrix of independent reactions (labeled $\boldsymbol{\nu}_I'$) is given by

$$\boldsymbol{\nu}_I'=\begin{bmatrix}1 & 1 & 1\\ 1 & 0 & 0\\ -1 & 1 & -1\end{bmatrix} \tag{A13}$$

hence $\boldsymbol{\phi}=\boldsymbol{\nu}_I'^T\boldsymbol{\Lambda}_{ASVD}$ where $\boldsymbol{\Lambda}_{ASVD}=\gamma_i$ ($i=1, 2, 3$). Note that using Eq. (19), it is obvious that $\boldsymbol{\Lambda}_{ASVD}$ is in the column space of $\boldsymbol{\nu}_I'$. Equating SVD and ASVD derived DoD vectors yields the desired linear relationship between the projections obtained from the SVD and ASVD models:

$$\boldsymbol{\nu}_I'^T\boldsymbol{\Lambda}_{ASVD}=\boldsymbol{A}_{SVD}^{-1}\boldsymbol{\Lambda}_{SVD} \tag{A14}$$

References

[1] Pope, S. B., and Ren, Z., 2009, "Efficient Implementation of Chemistry in Computational Combustion," Flow Turbul. Combust., **82**(4), pp. 437–453.

[2] Keck, J. C., and Gillespie, D., 1971, "Rate-Controlled Partial-Equilibrium Method for Treating Reacting Gas Mixtures," Combust. Flame, **17**(2), pp. 237–241.

[3] Keck, J. C., 1990, "Rate-Controlled Constrained-Equilibrium Theory of Chemical Reactions in Complex Systems," Prog. Energy Combust. Sci., **16**(2), pp. 125–154.

[4] Beretta, G. P., and Keck, J. C., 1986, "The Constrained Equilibrium Approach to Nonequilibrium Dynamics," Proceedings of the 1986 Winter Annual Meeting of the ASME, *Publ. Comput. Eng. Energy Syst. Second Law Anal. Model*, R. A. Gaggioli, ed., Anaheim, CA, Dec. 7–12, ASME B. H0341C-AES, vol. 3. pp. 135–139.

[5] Law, R., Metghalchi, M., and Keck, J. C., 1988, "Rate-Controlled Constrained Equilibrium Calculations of Ignition Delay Times in Hydrogen-Oxygen Mixtures," Proc. Combust. Inst., **22**(1), pp. 1705–1713.

[6] Bishnu, P., Hamiroune, D., Metghalchi, M., and Keck, J. C., 1997, "Constrained-Equilibrium Calculations for Chemical Systems Subject to Generalized Linear Constraints Using the NASA and STANJAN Equilibrium Programs," Combust. Theor. Model., **1**(3), pp. 295–312.

[7] Hamiroune, D., Bishnu, P., Metghalchi, M., and Keck, J. C., 1998, "Controlled Constrained Equilibrium Method Using Constraint Potentials," Combust. Theor. Model., **2**(1), pp. 81–94.

[8] Bishnu, P., Hamiroune, D., and Metghalchi, M., 2001, "Development of Constrained Equilibrium Codes and Their Applications in Nonequilibrium Thermodynamics," ASME J. Energy Resour. Technol., **123**(3), pp. 214–220.

[9] Ugarte, S., Gao, S., and Metghalchi, H., 2005, "Application of Maximum Entropy Principle in the Analysis of a Non-Equilibrium Chemically Reacting Mixture," Int. J. Thermodyn., **8**(1), pp. 43–53.

[10] Janbozorgi, M., Ugarte, S., Metghalchi, H., and Keck, J. C., 2009, "Combustion Modelling of Mono-Carbon Fuels Using the Rate-Controlled Constrained-Equilibrium Method," Combust. Flame, **156**(10), pp. 1871–1885.

[11] Janbozorgi, M., and Metghalchi, H., 2009, "Rate-Controlled Constrained-Equilibrium Theory Applied to the Expansion of Combustion Products in the Power Stroke of An Internal Combustion Engine," Int. J. Thermodyn., **12**(1), pp. 44–50.

[12] Janbozorgi, M., and Metghalchi, H., 2012, "Rate-Controlled Constrained-Equilibrium Modeling of H/O Reacting Nozzle Flow," J. Propul. Power, **28**(4), pp. 677–684.

[13] Beretta, G. P., Keck, J. C., Janbozorgi, M., and Metghalchi, H., 2012, "The Rate-Controlled Constrained-Equilibrium Approach to Far-From-Local-Equilibrium Thermodynamics," Entropy, **14**(2), pp. 92–130.

[14] Nicolas, G., Janbozorgi, M., and Metghalchi, H., 2014, "Constrained-Equilibrium Modeling of Methane Oxidation in Air," ASME J. Energy Resour. Technol., **136**(3), p. 032205.

[15] Nicolas, G., and Metghalchi, H., 2015, "Comparison Between RCCE and Shock Tube Ignition Delay Times At Low Temperatures," ASME J. Energy Resour. Technol., **137**(6), p. 062203.

[16] Nicolas, G., and Metghalchi, H., 2015, "Development of the Rate-Controlled Constrained-Equilibrium Method for Modeling of Ethanol Combustion," ASME J. Energy Resour. Technol., **138**(2), p. 022205.

[17] Yu, G., Metghalchi, H., Askari, O., and Wang, Z., 2019, "Combustion Simulation of Propane/Oxygen (With Nitrogen/argon) Mixtures Using Rate-Controlled Constrained-Equilibrium," ASME J. Energy Resour. Technol., **141**(2), p. 022204.

[18] Yu, G., Hadi, F., and Metghalchi, H., 2019, "Rate-Controlled Constrained-Equilibrium Application in Shock Tube Ignition Delay Time Simulation," ASME J. Energy Resour. Technol., **141**(2), p. 020801.

[19] Yu, G., Hadi, F., Wang, Z., and Metghalchi, H., 2019, "Review of Applications of Rate-Controlled Constrained-Equilibrium in Combustion Modeling," J. Non-Equil. Thermody., **45**(1), pp. 59–79.

[20] Hadi, F., Janbozorgi, M., Sheikhi, M. R. H., and Metghalchi, H., May 2013, "Assessment of Rate-Controlled Constrained-Equilibrium Method for Implementation of Detailed Kinetics in Turbulent Combustion Simulations," Proceedings of the 8th U.S. National Combustion Meeting, The Combustion Institute, Park City, UT.

[21] Yousefian, V., 1998, "A Rate Controlled Constrained Equilibrium Thermochemistry Algorithm for Complex Reacting Systems," Combust. Flame, **115**(1–2), pp. 66–80.

[22] Tang, Q., and Pope, S. B., 2004, "A More Accurate Projection in the Rate Controlled Constrained Equilibrium Method for Dimension Reduction of Combustion Chemistry," Combust. Theor. Model., **8**(2), pp. 255–279.

[23] Ren, Z., Pope, S. B., Vladimirsky, A., and Guckenheimer, J. M. J., 2007, "Application of the ICE-PIC Method for the Dimension Reduction of Chemical Kinetics Coupled with Transport," Proc. Combust. Inst., **31**(1), pp. 473–481.

[24] Hiremath, V., Ren, Z., and Pope, S. B., 2011, "Combined Dimension Reduction and Tabulation Strategy Using ISAT-RCCE-GALI for the Efficient Implementation of Combustion Chemistry," Combust. Flame, **158**(11), pp. 2113–2127.

[25] Jones, W. P., and Rigopolous, S., 2005, "Rate Controlled Constrained Equilibrium: Formulation and Application of Nonpremixed Laminar Flames," Combust. Flame, **142**(3), pp. 223–234.

[26] Løvås, T., Navarro-Martinez, S., and Rigopoulos, S., 2011, "On Adaptively Reduced Chemistry in Large Eddy Simulations," Proc. Combust. Inst., **33**(1), pp. 133–1346.

[27] Gorban, A. N., Karlin, I. V., Ilg, P., and Öttinger, H. C., 2001, "Corrections and Enhancements of Quasi-Equilibrium States," J. Non-Newt. Fluid Mech., **96**(1–2), pp. 203–219.

[28] Rigopoulos, S., and Løvås, T., 2009, "A LOI-RCCE Methodology for Reducing Chemical Kinetics, With Application to Laminar Premixed Flames," Proc. Combust. Inst., **32**(1), pp. 569–576.

[29] Hiremath, V., Ren, Z., and Pope, S. B., 2010, "A Greedy Algorithm for Species Selection in Dimension Reduction of Combustion Chemistry," Combust. Theor. Model., **14**(5), pp. 619–652.

[30] Rena, Z., Lu, Z., Gao, Y., Lu, T., and Hou, L., 2017, "A Kinetics-Based Method for Constraint Selection in Rate-Controlled Constrained Equilibrium," Combust. Theory Model., **21**(2), pp. 159–182.

[31] Hadi, F., Yousefian, V., Sheikhi, M. R. H., and Metghalchi, H., 2016, "A Study of the RCCE Constraint Potential Formulation Incorporating a Constraint Selection Algorithm," Proceedings of the 2016 ESSCI Spring Meeting, Princeton, NJ, March.

[32] Hadi, F., Yousefian, V., Sheikhi, M. R. H., and Metghalchi, H., 2017, "Time Scale Analysis for Rate-Controlled Constrained-Equilibrium Constraint Selection," Proceedings of the 10th U.S. National Combustion Meeting of the Combustion Institute, College Park, MD, April.

[33] Beretta, G. P., Janbozorgi, M., and Metghalchi, H., 2016, "Degree of Disequilibrium Analysis for Automatic Selection of Kinetic Constraints in the Rate-Controlled Constrained-Equilibrium Method," Combust. Flame, **168**, pp. 342–364.

[34] Rivadossi, L., and Beretta, G. P., 2016, "Validation of the ASVDADD Constraint Selection Algorithm for Effective RCCE Modeling of Natural Gas Ignition in Air," Proceedings of IMECE2016—the ASME 2016 International Mechanical Engineering Congress and Exposition, Phoenix, Arizona, IMECE2016.

[35] Beretta, G. P., Rivadossi, L., and Janbozorgi, J., 2018, "Systematic Constraint Selection Strategy for Rate-Controlled Constrained-Equilibrium Modeling of Complex Nonequilibrium Chemical Kinetic," J. Non-Equil. Thermody., **43**(2), pp. 121–130.

[36] Hadi, F., Yousefian, V., Sarfaraz, E., and Beretta, G. P., 2018, "Extending Degree of Disequilibrium Analysis for Automatic Selection of Kinetic Constraints in the Rate-Controlled Constrained-Equilibrium Method," Proceedings of the 2018 ASME International Mechanical Engineering Congress & Exposition, Pittsburgh, PA, IMECE2018.

[37] Roy, S., Hadi, F., and Askari, O., 2019, "Rate-Controlled Constrained-Equilibrium Simulation of Ethanol Combustion Using SVD Derived Constraints," Proceedings of the 2019 ASME International Mechanical Engineering Congress & Exposition, Salt Lake City, UT, IMECE2019.

[38] Hadi, F., Janbozorgi, M., Sheikhi, M. R. H., and Metghalchi, H., 2016, "A Study of Interactions Between Mixing and Chemical Reaction Using the Rate-Controlled Constrained-Equilibrium Method," J. Non-Equil. Thermody., **41**(4), pp. 257–278.

[39] PourMohamadHadiFarshami, F., 2016, "Rate-Controlled Constrained-Equilibrium Modeling of Chemical Kinetics and Mixing," Ph.D. Thesis, Northeastern University, Department of Mechanical and Industrial Engineering, Boston Massachusetts.

[40] Hadi, F., Yu, G., and Metghalchi, H., 2018, "Fundamentals of Rate-Controlled Constrained-Equilibrium Method," *Energy for Propulsion, Green Energy and Technology*, Runchal, A., Gupta, A., Kushari, A., De, A., Aggarwal, S., eds., Springer, Singapore, pp. 237–266, Ch 10.

[41] Hadi, F., and Sheikhi, M. R. H., 2015, "A Comparison of Constraint and Constraint Potential Forms of the Rate-Controlled Constrained-Equilibrium Method," ASME J. Energy Resour. Technol., **138**(2), p. 022202.

[42] Beretta, G. P., 2009, "Nonlinear Quantum Evolution Equations to Model Irreversible Adiabatic Relaxation with Maximal Entropy Production and Other Nonunitary Processes," Rep. Math. Phys., **64**(1–2), pp. 139–168.

[43] Martin, C., and Porter, M. A., 2012, "The Extraordinary SVD," Am. Math. Monthly, **119**(10), pp. 838–851.

[44] Rivadossi, L., and Beretta, G. P., 2018, "Validation of the ASVDADD Constraint Selection Algorithm for Effective RCCE Modeling of Natural Gas Ignition in Air," ASME J. Energy Resour. Technol., **140**(5), p. 052201.